New U-Pb age constraints at Freegold Mountain: Evidence for multiple phases of polymetallic mid- to Late Cretaceous mineralization

Thierry Bineli Betsi[1]
University of New Brunswick

Venessa Bennett[2]
Yukon Geological Survey

Bineli Betsi, T. and Bennett, V., 2010. New U-Pb age constraints at Freegold Mountain: Evidence for multiple phases of polymetallic mid- to Late Cretaceous mineralization. *In*: Yukon Exploration and Geology 2009, K.E. MacFarlane, L.H. Weston and L.R. Blackburn (eds.), Yukon Geological Survey, p. 57-84.

ABSTRACT

In this contribution, we present new U-Pb age data for ten intrusive units that bracket the timing of polymetallic mineralization occurring within the Northern Freegold Resources Ltd. (NFR), Freegold Mountain project area. Polymetallic mineralization occurring in the Tinta zone predates trachytic dykes (~109 Ma) and represents the earliest phase of mineralization recognized on the Freegold Mountain property thus far. Feldspar porphyry dykes that intrude the Revenue zone are correlative to the Nucleus zone feldspar porphyry dykes, and yield ages of ~105-104 Ma, indicating that the structural corridor in which Au mineralization occurred was active from at least this time. Furthermore, monzodiorite was emplaced at ~107 Ma within the Revenue zone. An ~97 Ma aplitic dyke that intrudes porphyritic granite of the Stoddart intrusion predates ~94 Ma Mo-Cu-W mineralization. Andesitic dykes (~77 Ma) that crosscut the Stoddart porphyry and rhyolitic dykes (~75 Ma) intruding the Revenue zone, represent Carmacks-age volcanism in the region. These new age data indicate that economically important mineralizing events took place over a period of at least 40 Ma.

[1]*thierry.bineli@unb.ca*

[2]*venessa.bennett@gov.yk.ca*

INTRODUCTION

The Freegold Mountain project, owned and operated by Northern Freegold Resources Ltd., is located in the central Dawson Range, west central Yukon. The property is situated at the southern end of a regionally extensive, northwest-trending polymetallic mineral belt associated with Jurassic to latest Cretaceous magmatic events (Figs. 1, 2). The Freegold Mountain property represents a large land parcel exceeding 12 000 hectares and is host to numerous important mineralized zones, including two with NI 43-101 resources, *i.e.*, the Tinta deposit (*Au-Ag-Cu-Pb-Zn*) and the Nucleus Au deposit. Significant zones of mineralization currently recognized across the property include, from northwest to southeast, Nitro, Big, Nucleus, Revenue, Castle, Discovery (Ridge and Stoddart), Goldy and Tinta (Fig. 3). Each mineralized zone is associated with a different metal suite of interest, and corresponding style and setting of mineralization. The density of such diverse styles of mineralization in a relatively small area suggests a complex interplay of long-lived structural conduits and multiphase fertile magmatism. The following report presents new U-Pb age data from the Tinta, Revenue, Stoddart and Ridge mineralized zones that demonstrate a protracted history of polymetallic mineralization extending for over 40 Ma that was associated with discrete pulses of Cretaceous magmatism. Importantly, these new age data place maximum and minimum age constraints on the timing of mineralization occurring across the Freegold Mountain project area.

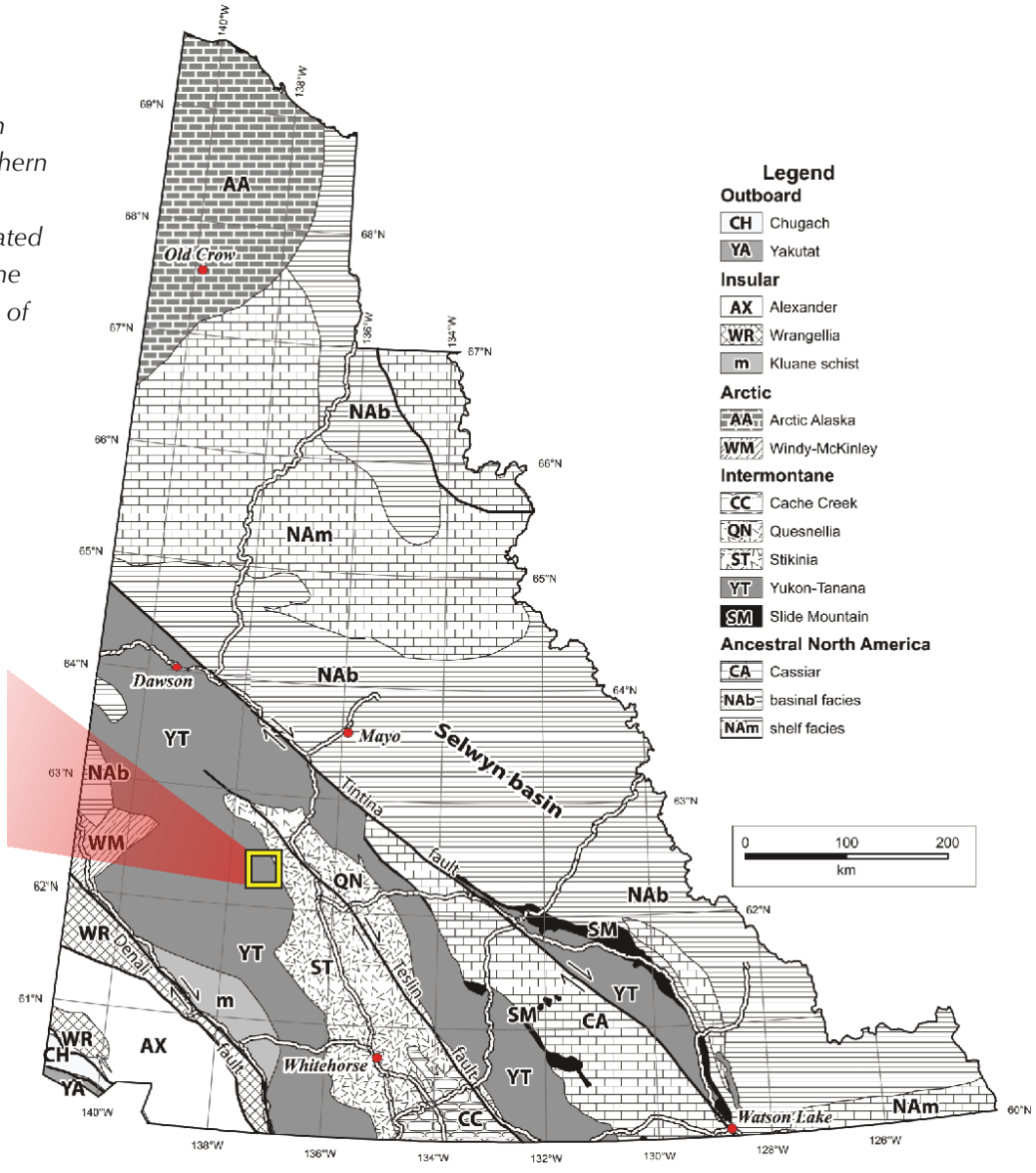

Figure 1. *Terrane map of Yukon illustrating the location of Northern Freegold Resources' Freegold Mountain project, which is located west of the Teslin fault within the Yukon-Tanana terrane (courtesy of M. Colpron).*

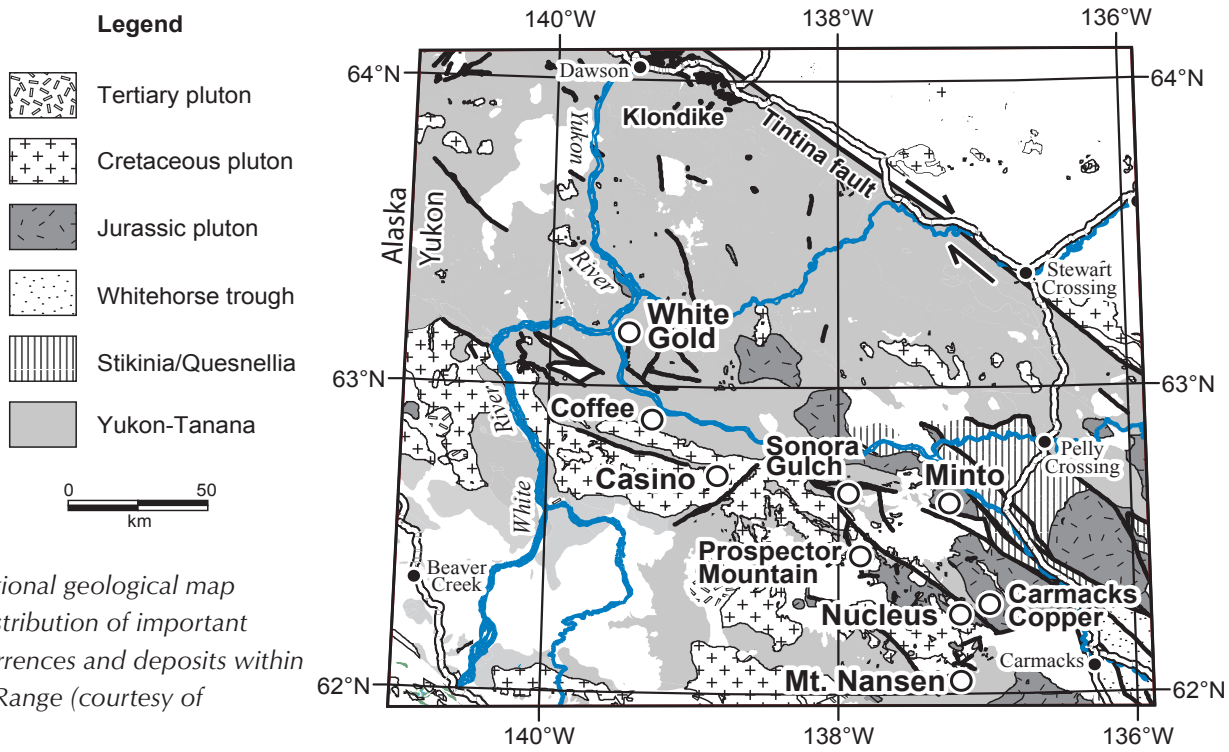

Figure 2. *Regional geological map illustrating distribution of important mineral occurrences and deposits within the Dawson Range (courtesy of M. Colpron).*

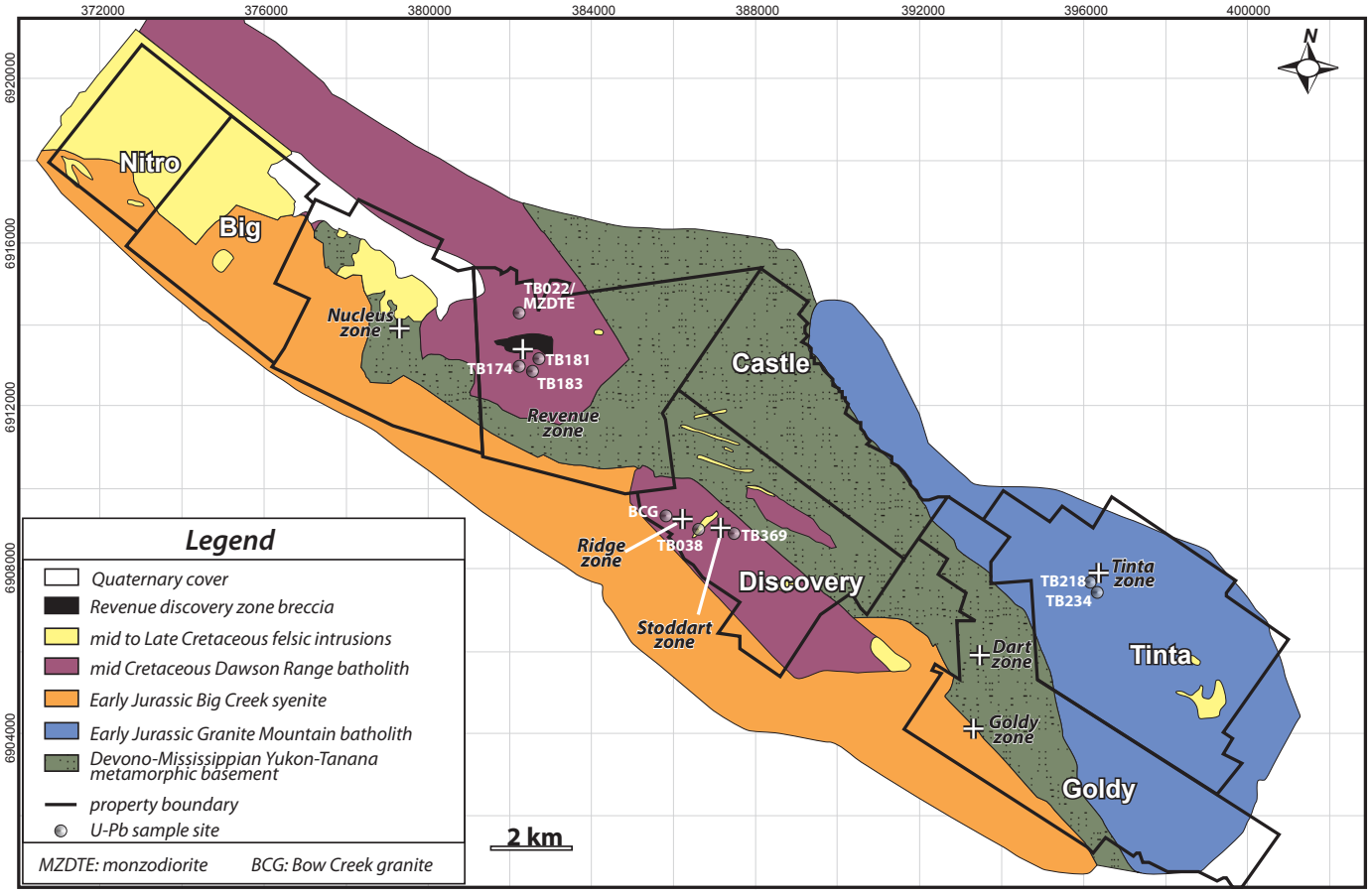

Figure 3. *Property geology map of Freegold Mountain project, 2009 (Northern Freegold Resources Ltd.); location of U-Pb sampling sites are noted.*

REGIONAL GEOLOGY

The Freegold Mountain project is located within the Dawson Range (Fig. 2), which is bounded primarily by the Yukon River to the north and the Nisling River to the south. It extends west-northwesterly from the town of Carmacks to the White River. The Dawson Range is underlain, in part, by Paleozoic metasedimentary and metaplutonic rocks of the pericratonic Yukon-Tanana terrane (YTT), which represents a composite of terranes that were accreted to the North American continent during early Mesozoic time (Colpron *et al.*, 2006). Regional metamorphic grade varies from greenschist to lower amphibolite facies (Payne *et al.*, 1987). The YTT has been intruded by several different phases of plutonic rocks of at least three different ages. More than one terminology has been introduced in the literature for some of the different suites and specific intrusions in the Dawson Range. The following nomenclature is recommended.

1. Early Jurassic Aishihik and Long Lakes suites (Johnston, 1995)

- Big Creek Metaplutonic Suite (Carlson, 1987) or Big Creek syenite (Tempelman-Kluit, 1984): orthoclase-hornblende porphyritic syenite, plagioclase-hornblende monzonite, and hornblendite
- Granite Mountain batholith (Tempelman-Kluit, 1984; Carlson, 1987): foliated coarse-grained hornblende-biotite granodiorite and leucogranodiorite

2. Mid-Cretaceous Whitehorse Plutonic Suite (Gordey and Makepeace, 2000)

- Dawson Range batholith (Tempelman-Kluit, 1974): hornblende-biotite-quartz diorite, hornblende-biotite diorite, and biotite-hornblende granodiorite
- Coffee Creek granite (Carlson, 1987): granite to quartz monzonite
- Casino granodiorite (Gordey and Makepeace, 2001)

3. Late Cretaceous Prospector Mountain Suite (Johnston, 1995)

- Casino Plutonic Suite (Johnston, 1995): leucocratic granite, quartz monzonite and alaskite with associated aplite phases
- Bow Creek granite (Carlson, 1987): biotite granite and related quartz-feldspar porphyry dykes
- Seymour Creek stock (McCausland *et al.*, 2001): biotite-hornblende granodiorite to quartz monzonite
- Middle and Late Cretaceous volcanic sequences and associated hypabyssal dykes belong to the Mount Nansen and Carmacks groups respectively (Carlson, 1987)

Late Cretaceous plutons in the Dawson Range are thought to have been derived through subduction processes and melt generation within the mantle, whereas mid-Cretaceous intrusions were generated through partial melting of the YTT basement (Selby *et al.*, 1999). The Big Creek fault is a prominent northwest-trending topographic and aeromagnetic feature of regional extent that extends across the Freegold Mountain project area. Importantly, the Big Creek fault zone is the locus of numerous copper porphyry and structurally hosted gold deposits, as well as associated placer gold. Mid and Late Cretaceous pluton emplacement may have been localized by the presence of these major northwest-trending structures.

FREEGOLD MOUNTAIN PROJECT - PROPERTY GEOLOGY

Poly-deformed and metamorphosed metagranitic, metavolcanic, and subordinate metasedimentary rocks of probable Devonian to Mississippian and older ages comprise the YTT basement that underlies the Freegold Mountain project area. The metamorphic assemblage has been intruded by four regional magmatic suites including, (i) the early Jurassic Granite Mountain batholith, located in the southeast margin of the property; (ii) the early Jurassic Big Creek syenite, which parallels the southwest property boundary and locally occurs in the south-central region of the property; (iii) the mid to Late Cretaceous Dawson Range batholith that underlies Revenue, and parts of the Nucleus and Discovery zones; and (iv) mid and Late Cretaceous intrusions and volcanic rocks of the Mount Nansen volcanic suite that partly underlie the Nitro and Big zones. The Big Creek lineament parallels Big Creek, which anastomoses in a general west-northwest trend across the Freegold Mountain property. The Big Creek lineament is interpreted to represent an important structure for controlling pluton emplacement and associated mineralization. Here, we provide more details on the geological setting for the Tinta, Revenue, Stoddart and Ridge mineralized zones for which U-Pb geochronology samples were collected.

TINTA ZONE

The Tinta zone is underlain by early Jurassic granodiorite, quartz monzonite and minor hornblendite of the Granite Mountain batholith and, locally, small lenses of amphibolites of the YTT basement (Fig. 3). Early Jurassic plutonic rocks within the Tinta zone are crosscut by two phases of dykes including pink, equigranular aplite dykes and dark green to black, quartz-feldspar porphyry dykes of trachytic composition. Samples of both dyke suites were collected to constrain maximum and minimum ages of mineralization within the Tinta zone. Tinta zone mineralization represents a structurally controlled, northwest-trending polymetallic (Cu-Zn-Pb-As-Ag-Au) vein system. Mineralization occurs as quartz-pyrite-rich, base-metal-bearing Au-Ag vein systems (Fig. 4). Sulphide phases include chalcopyrite, galena and sphalerite (Fig. 4). Silver-bearing minerals include tennantite and/or tetrahedrite, in addition to galena. The mineralized vein is typically zoned and composed of a marginal pyritic zone, and a central zone comprising mostly base metals and rare sulfosalts (Fig. 4b). Locally, base-metal mineralization is zoned into a peripheral chalcopyrite zone, and an interior galena-sphalerite zone (Fig. 4b). Alteration mineral assemblages that include quartz-sericite-adularia-carbonate and open-space colloform and comb quartz textures are indicative of a high-level vein emplacement; this is consistent with an epithermal designation for the Tinta deposit.

REVENUE AND NUCLEUS ZONES

Historically, the Revenue and Nucleus mineralized zones were considered as a single property, termed Golden Revenue (Eaton, 1984), but are now recognized as discrete and different mineralized zones that include the NI 43-101 Nucleus Au Deposit (Inferred resource of 1,082,000 ounces of gold at 0.50 g/t Au with a cutoff of 0.3 g/t) and the Au ± Cu prospect of the Revenue zone (Fig. 3). We describe the geology and mineralization of the Nucleus and Revenue zones together in this study due to the likely continuation of the structural corridor hosting

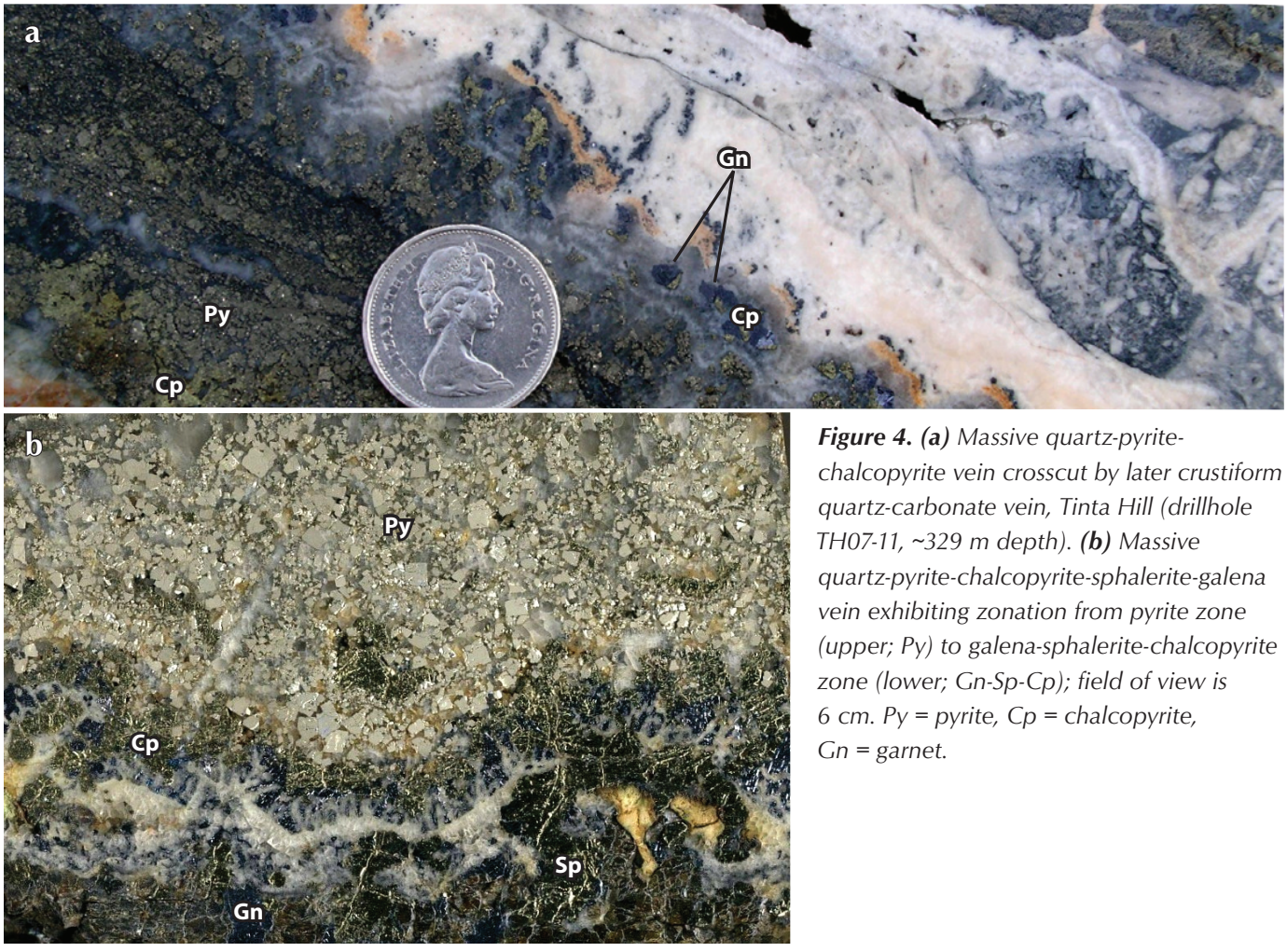

Figure 4. ***(a)*** *Massive quartz-pyrite-chalcopyrite vein crosscut by later crustiform quartz-carbonate vein, Tinta Hill (drillhole TH07-11, ~329 m depth).* ***(b)*** *Massive quartz-pyrite-chalcopyrite-sphalerite-galena vein exhibiting zonation from pyrite zone (upper; Py) to galena-sphalerite-chalcopyrite zone (lower; Gn-Sp-Cp); field of view is 6 cm. Py = pyrite, Cp = chalcopyrite, Gn = garnet.*

Nucleus-style mineralization into the Revenue zone, as well as the occurrence of Nucleus-style feldspar porphyry dykes within the Revenue zone.

Basement rocks of the Nucleus and Revenue zones consist predominantly of strongly deformed, locally mylonitic, metasedimentary and meta-igneous schistose and gneissose rocks of the YTT that are intruded by early Jurassic, mid and Late Cretaceous intrusive bodies. Intrusive units intruding the Nucleus and Revenue zones are compositionally diverse and consist of the following:

i. medium-grained, unfoliated and equigranular leucogranite (Nucleus and Revenue);

ii. fine-grained, foliated and unfoliated, locally porphyritic leucomicrogranite (Nucleus and Revenue);

iii. medium to coarse-grained, locally porphyritic alkali leucogranite (Revenue);

iv. white-brown weathering, equigranular and pervasively chloritized biotite-hornblende granite and homogeneous, locally foliated biotite granite (Revenue);

v. mesocratic, medium-grained hornblende-biotite monzonite to quartz monzonite (Revenue); and

vi. weakly deformed monzodiorite-monzogabbro (Revenue).

The youngest intrusions identified through observation of overprinting relationships in both the Revenue and Nucleus zones include aplitic and dacitic to rhyolitic porphyry dyke swarms. In addition, a high-level intrusive breccia, referred to as tuffisite, has also intruded the composite plutonic basement, described above, that underlies the Revenue zone. The tuffisite consists of angular to subrounded lithic clasts of quartz-feldspar porphyry and subordinate, variably altered granitic and metasedimentary clasts hosted in a crystal-rich quartz-feldspar matrix. Four trachydacitic to rhyolitic porphyry dykes from the Revenue zone were sampled to determine a crystallization age.

Despite the initial classification as a porphyry Cu-Mo-Au target, the Nucleus Deposit has been reinterpreted on the basis of detailed drilling as a structurally controlled, telescoped magmatic hydrothermal system. Mineralization styles include Au-enriched, mesothermal sulphide-calc-silicate replacement bodies (Fig. 5a); Au-Cu quartz stockworks and associated veining (Fig. 5b); sheeted veins and breccias (Fig. 5c and d respectively); and epithermal crustiform veins in addition to mineralized feldspar porphyry dykes (Fig.5d). Oriented diamond drilling indicates that Nucleus mineralization is oriented east-west, as defined by geometry of both the feldspar porphyry dyke swarm and vein-hosted styles of mineralization. Overprinting relationships in the Nucleus Au Deposit demonstrate a progression from deeper level, early-formed porphyry, skarn and replacement styles of mineralization, to higher level, likely epithermal mineralization, that are inferred to be associated with both the Mt. Nansen and Carmacks magmatic events.

Significant mineralization currently recognized in the Revenue zone consists of the initial Revenue discovery zone breccia pipe (tuffisite) that has significant supergene copper mineralization (malachite-azurite-gypsum/anhydrite; Fonseca, 2009; Fig. 5e and f). Sulphide copper mineralization is observed in both the clasts and the matrix of the intrusive breccia. Preferential mineralization occurs in Fe-bearing clasts by the process of sulfidation reactions, and by pyrite ± chalcopyrite formation within the crystal-rich matrix.

DISCOVERY ZONE – STODDART AND RIDGE

The polymetallic Ridge and Stoddart porphyry mineralized deposits represent the two main targets occurring within the Discovery zone, which is comprised of several intrusive bodies including a series of dyke swarms of basaltic-andesitic (Ridge) and aplitic (Stoddart) compositions. Four main intrusive bodies are recognized within the Discovery zone including an equigranular, medium-grained, hornblende-biotite-magnetite granite; a strongly magnetic alkali feldspar porphyritic granite; a pink, medium-grained granite with distinctive hornblende-biotite aggregates (Bow Creek granite); and a medium-grained, melanocratic biotite monzonite.

Porphyry-style Cu-Mo-W mineralization at the Stoddart zone occurs as both quartz-chalcopyrite-molybdenite-scheelite veins and microstockwork, as well as a sub-parallel set of veins, or as chalcopyrite-molybdenite-scheelite disseminations (Fig. 6a and c). Additionally, mineralization is observed to be associated with either phyllic (quartz-sericite), or potassic (K-feldspar-biotite-magnetite after primary biotite) alteration. A Re-Os isotopic age date of molybdenite sampled from the Stoddart zone mineralization yielded a model age of 93.6 ± 1.5 Ma (Geospec Consultants Ltd., 2008).

Polymetallic Au-Ag-Pb-Cu mineralization occurring within the Ridge zone is hosted by a northwest-trending shear zone approximately 5 m to 10 m wide (apparent), located

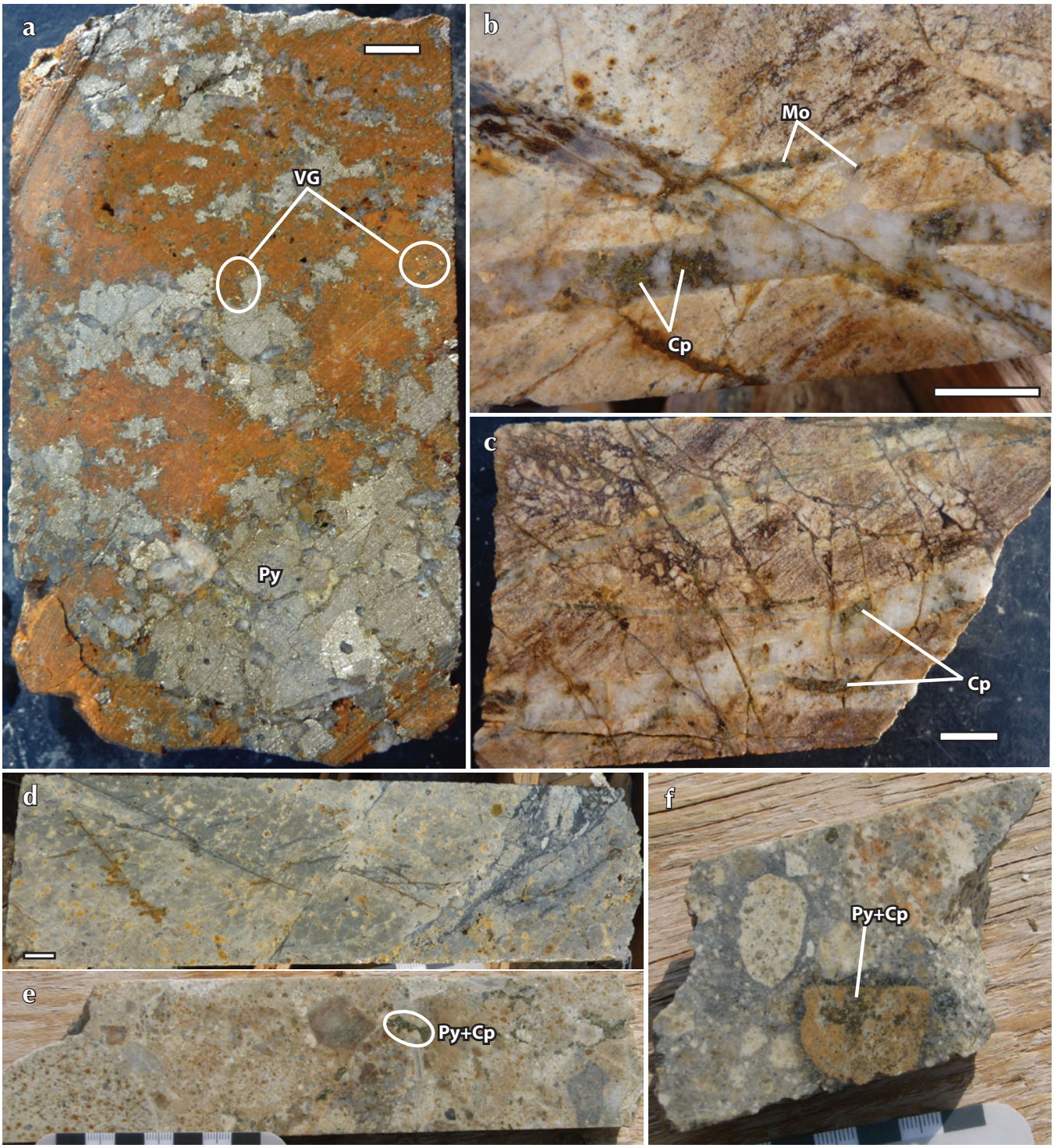

Figure 5. ***(a)*** *High-grade, gold-copper skarn, Nucleus zone. Visible gold (VG) occurs in early phase assemblage (quartz-feldspar-biotite) and is overprinted by pyrrhotite-chalcopyrite-pyrite.* ***(b)*** *Quartz-chalcopyrite-molybdenite stockwork mineralization, Nucleus zone.* ***(c)*** *Quartz stockwork mineralization overprinted by late-stage brittle veining and brecciation, Nucleus zone.* ***(d)*** *Example of silicified feldspar porphyry dyke with overprinting brittle deformation and brecciation, Nucleus zone.* ***(e)*** *Matrix mineralization of pyrite and chalcopyrite (Py + Cp) occurring within tuffisite unit, Revenue zone.* ***(f)*** *Clast-hosted sulphide mineralization (Py + Cp), tuffisite, Revenue zone. Scale card increments and scale bars in Figures 5 a-f represent 1 cm. Py = pyrite, Mo = molybdenite, Cp = chalcopyrite.*

at, or near, the contact of a strongly foliated biotite granodiorite and the Bow Creek granite. Early-phase copper and gold mineralization occurs as malachite, azurite, chalcocite, and/or telluride, with gold. Dolomitic veining represents late-stage overprinting and exhibits crustiform textures that locally host galena mineralization (Fig. 7a-d). Dolomite veining parallels the southeast-trend of the shear zone, and crosscuts the biotite monzonite (Fig. 7a) and Bow Creek granite.

GEOCHRONOLOGY

Ten magmatic samples were collected from surface and drill core from the Tinta, Revenue, Stoddart and Ridge mineralized zones for U-Pb dating. Sampling was restricted to magmatic phases, which were either directly associated with mineralization, or were observed to postdate it. Dating was completed using both U-Pb Isotope Dilution Thermal Ionization Mass Spectrometry (ID-TIMS; 7 samples) and Laser Ablation Microprobe Inductively Coupled Plasma-Mass Spectometry (LAM ICP-MS; 3 samples) techniques. The samples are reported

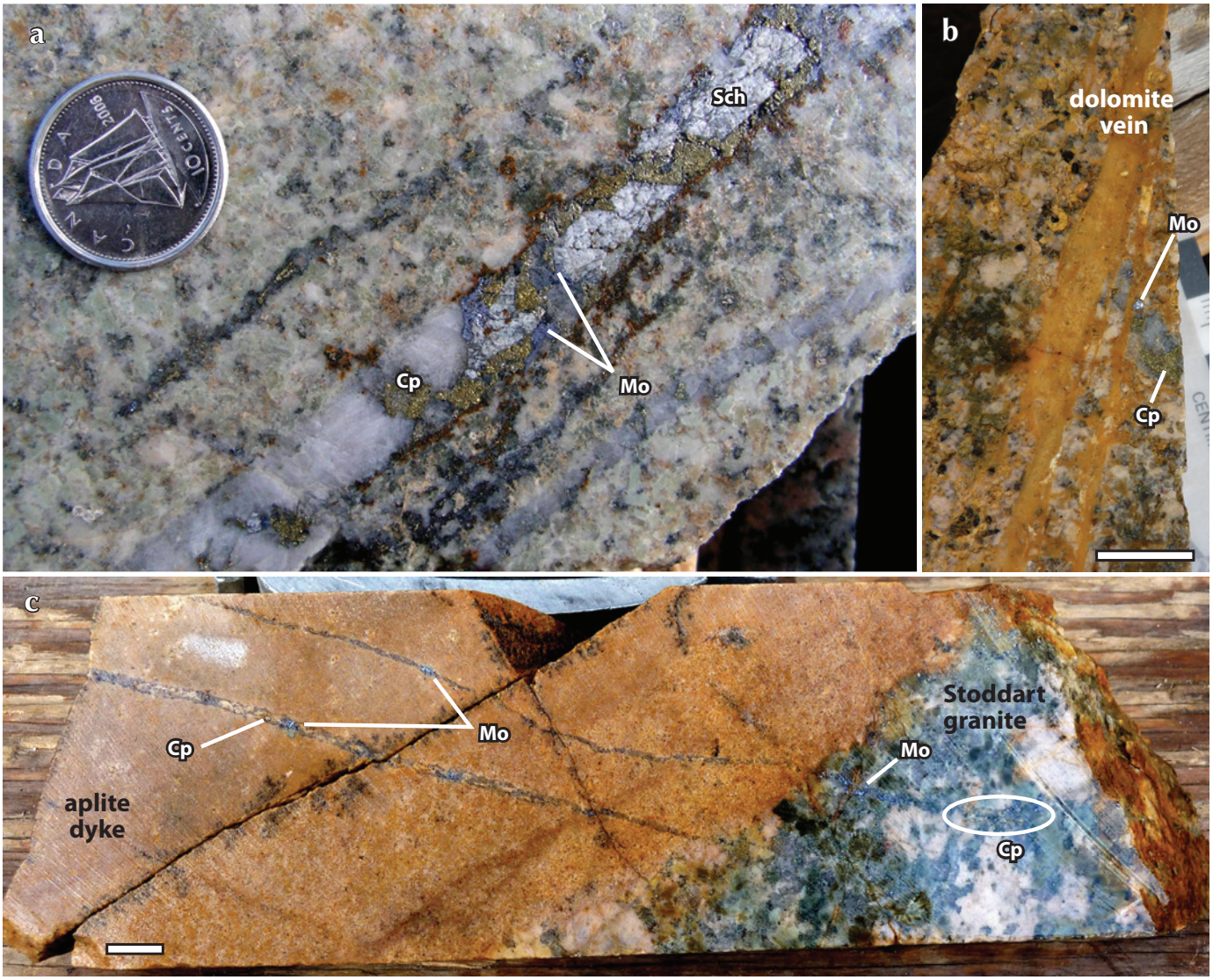

Figure 6. ***(a)*** *Quartz-scheelite-chalcopyrite-molybdenite vein crosscutting granite and overprinted by phyllic (sericite-quartz) alteration (drillhole 08 ST07, at 180 m).* ***(b)*** *Quartz-chalcopyrite-molybdenite mineralization within Stoddart zone granite overprinted by late-stage dolomitic veining.* ***(c)*** *Quartz-chalcopyrite-molybdenite veins crosscutting aplitic dyke that intrudes Stoddart pluton. Aplite dyke is equivalent to TB369 sampled for U-Pb age dating. Scale bars represent 1 cm. Cp = chalcopyrite, Mo = molybdenite, Sch = scheelite.*

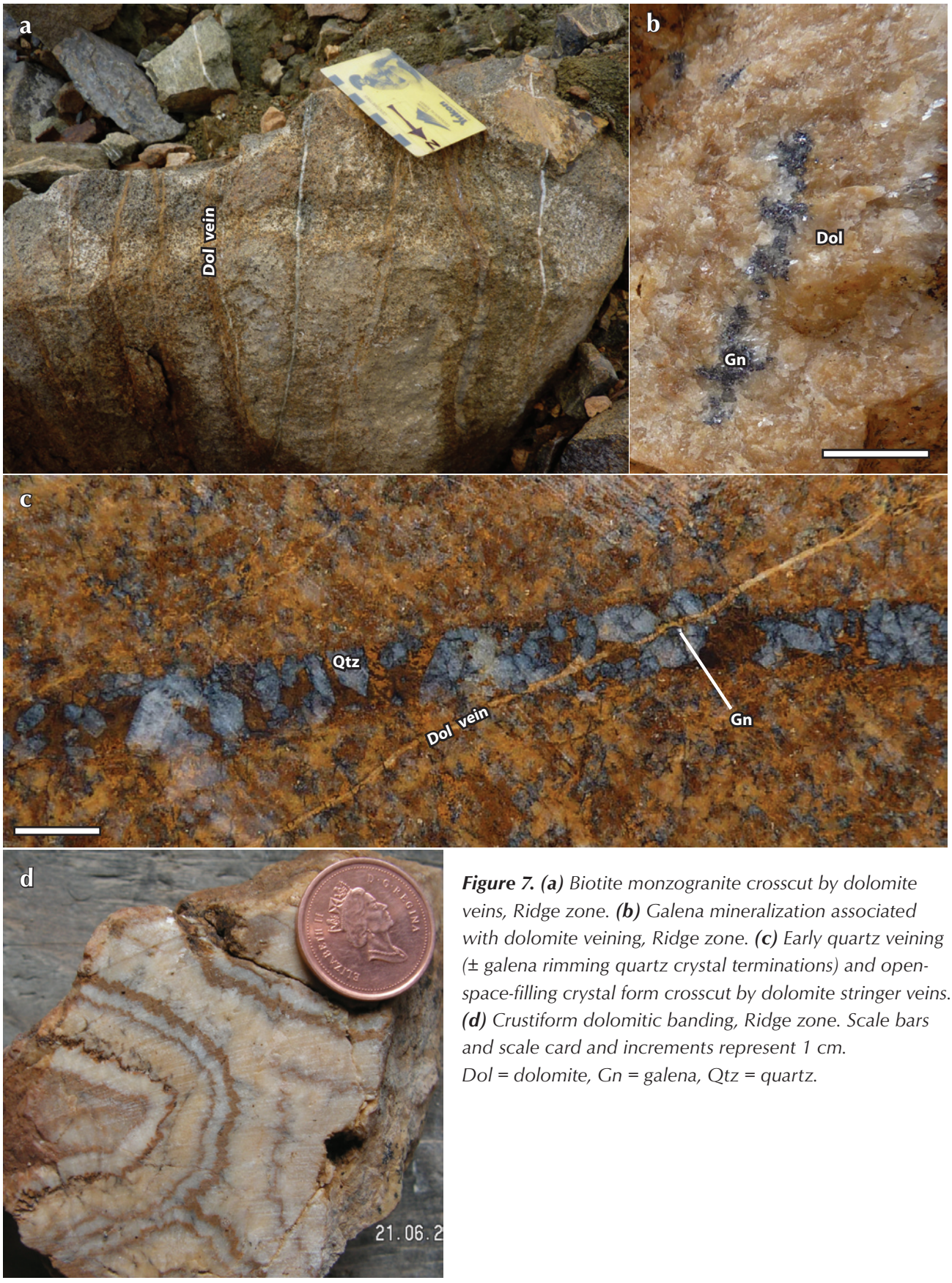

Figure 7. ***(a)*** *Biotite monzogranite crosscut by dolomite veins, Ridge zone.* ***(b)*** *Galena mineralization associated with dolomite veining, Ridge zone.* ***(c)*** *Early quartz veining (± galena rimming quartz crystal terminations) and open-space-filling crystal form crosscut by dolomite stringer veins.* ***(d)*** *Crustiform dolomitic banding, Ridge zone. Scale bars and scale card and increments represent 1 cm.*
Dol = dolomite, Gn = galena, Qtz = quartz.

Table 1. *Summary of crystallization ages, Freegold Mountain project.*

Zone	Sample	$^{206}Pb/^{238}U$ weighted mean age
Tinta	TB234	unresolved
	TB218	108.7 ± 0.4 Ma
Revenue	TB183	105.7 ± 0.2 Ma
	TB022	105.5 ± 0.2 Ma
	TB174	104.4 ± 0.1 Ma
	TB181	75.2 ± 0.2 Ma
	Revenue Creek granite	107.1 ± 0.6 Ma
Stoddart Re-Os Mo (94Ma)	TB369 (Concordia age)	97.9 ±0.4 Ma
	TB038	76.9 ± 0.9 Ma
Ridge	Bow Creek granite	68.4 ± 0.9 Ma

according to the mineralized zone in which they were sampled and, where possible, sequentially presented from oldest to youngest. Final calculated ages are reported in Table 1.

Conventional and chemical abrasion ID-TIMS zircon U-Pb dating was performed at the Pacific Centre for Isotope and Geochemical Research (PCIGR) of the University of British Columbia. Analytical techniques for U-Pb dating studies by ID-TIMS at the PCIGR are as described by Mortensen *et al.* (1995). Interpreted crystallization ages are based on a weighted average of the $^{206}Pb/^{238}U$ ages calculated for at least two overlapping concordant points. Errors for the calculated concordia and weighted mean $^{206}Pb/^{238}U$ ages are given at the 2 sigma level. Field relationships are briefly described for each sample before reporting the U-Pb IDTIMS isotopic results.

Three samples from the Freegold Mountain property were dated using U-Pb LAM ICP-MS techniques at the INCO Innovation Centre at Memorial University, St. Johns, Newfoundland. A detailed outline of the methodology is given in Bennett and Tubrett (this volume). Analytical techniques to characterize the zircon populations included standard optical microscopy and backscattered electron imaging (BSE) and cathodoluminescence (CL) image analysis in order to permit greater understanding of zircon zoning and growth history. Image analysis was completed on all zircon grains selected (n = 20 to 80, dependent on yield). Field relationships and zircon zonation styles are briefly described for each sample before reporting the U-Pb isotopic results. Uncertainties reported for all calculated ages and plotted on associated concordia and weighted mean diagrams are at the 2σ uncertainty level, unless stated otherwise. Final age calculations include U-decay constant uncertainties, which are plotted graphically on concordia plots. Concordia and weighted mean $^{206}Pb/^{238}U$ ages were calculated using Ludwig (1999). The concordia age that includes U-decay constant uncertainties is considered the best estimate of the crystallization age of a sample (see Bennett and Tubrett, this volume). Where a concordia age has a mean square of weighted deviates (MSWD) >1.5, the weighted mean $^{206}Pb/^{238}U$ age is considered the best estimate of the crystallization age. Uranium and Th concentration data and Th/U ratios were also calculated for each sample.

TINTA ZONE

One porphyry dyke and one aplite dyke were sampled from the Tinta mineralized zone, TB218 and TB234, respectively. The porphyry dyke was observed to crosscut polymetallic mineralization, whereas the aplite dyke hosts mineralization.

Sample TB218 is a dark green to black feldspar porphyritc dyke of trachytic composition sampled from DDH TH 07-08 between intervals 38.45 m and 38.65 m. The dyke has strong pervasive chlorite-epidote alteration of both phenocrysts and groundmass. The sample TB218 dyke intrudes hornblende-granodiorite of assumed Jurassic age, and is possibly associated with the Granite Mountain batholith. Additionally, carbonate veining is observed crosscutting the dyke, and represents a later overprinting fluid system.

Three single-grain zircon fractions were analysed from sample TB218 by conventional ID-TIMS (Table 2; Fig. 8a). Three overlapping concordant data points yielded a concordia age of 108.7 ± 0.17 Ma (MSWD = 0.25) and a weighted mean $^{206}Pb/^{238}U$ age of 108.7 ± 0.36, which is interpreted to be the crystallization age of TB218 (Fig. 8b).

Sample TB234 is a pink, equigranular aplitic dyke sampled from DDH TH 07-11, at 188.1 m. The dyke intrudes granodiorite of the Granite Mountain batholith and is comprised dominantly of feldspars (~80 vol. %) exhibiting poikiolitic textures and subordinate quartz (~20 vol. %). Locally, feldspar is altered to saussurite, carbonate and clay minerals. Five single-grain zircon fractions were analysed from TB234 (Table 2; Fig. 8c). No overlapping concordant points occur in the dataset, and calculated $^{206}Pb/^{238}U$ ages range from *ca.* 188 Ma to 216 Ma. The

most reasonable interpretation of the isotopic variability in the dataset is that the zircon fractions analysed represent inherited populations. Further work is required to establish the crystallization age of this sample.

REVENUE ZONE

Four feldspar porphyry dykes (TB022, TB174, TB183, TB181) and one monzodiorite intrusion (Revenue Creek monzodiorite) were sampled in the Revenue zone. The porphyry dykes are interpreted to be correlative to the mineralizing porphyry dykes that occur in the Nucleus zone. The porphyry dykes were analysed using conventional ID-TIMS, whilst U-Pb dating of the Revenue Creek monzodiorite was done using LAM ICP-MS.

Sample TB022 was collected in Revenue Creek, immediately adjacent to Revenue Camp (382254E, 6914428N). The dyke is rhyolitic in composition and contains approximately 5% modal quartz and feldspar phenocrysts set in an aphanitic groundmass composed almost entirely of quartz. Strong pervasive silicification and weak to moderate pyrite ± chalcopyrite mineralization is also associated with TB022. Importantly, the feldspar porphyry dyke crosscuts the Revenue Creek monzodiorite. Immediately proximal to the dyke contacts, strong biotite alteration is observed, which is associated

Table 2. *Conventional U-Pb ID-TIMS data for zircon fractions from porphyritic dykes from Tinta and Revenue zones.*

sample/ fraction	$^{207}Pb/^{235}U$ ratio	± 1σ, %	$^{206}Pb/^{238}U$ ratio	± 1σ, %	rho	$^{206}Pb/^{238}U$ age	± 2σ, Ma	$^{207}Pb/^{235}U$ age	± 2σ, Ma	$^{207}Pb/^{206}Pb$ age	± 2σ, Ma
TB234 Tinta											
A	0.2212	0.1700	0.0314	0.0920	0.8025	199.3	0.4	202.9	0.6	244.5	5.1/5.1
B	0.2343	0.1980	0.0332	0.0720	0.6243	210.4	0.3	213.7	0.8	250.4	7.5/7.5
C	0.2033	0.2390	0.0296	0.0810	0.6012	188.0	0.3	187.9	0.8	187.8	9.3/9.4
D	0.2372	0.2560	0.0338	0.0950	0.5224	214.1	0.4	216.2	1.0	238.7	10.2/10.2
E	0.2197	1.5250	0.0315	0.1530	0.6047	199.7	0.6	201.7	5.6	224.9	65.1/67.8
TB218 Tinta											
A	0.1130	0.3500	0.0170	0.1130	0.4963	108.6	0.2	108.7	0.7	111.3	14.6/14.7
B	0.1132	0.1630	0.0170	0.0810	0.6510	108.8	0.2	108.9	0.3	111.8	5.9/6.0
C	0.1127	0.2430	0.0170	0.1400	0.4494	108.5	0.3	108.4	0.5	108.1	10.3/10.4
TB183 Revenue											
A	0.1090	1.1720	0.0165	0.1420	0.5589	105.6	0.3	105.0	2.3	92.8	51.3/52.9
B	0.1100	1.0710	0.0165	0.1900	0.4424	105.8	0.4	106.0	2.2	110.6	46.6/48.0
C	0.1104	0.8830	0.0166	0.1690	0.4619	105.8	0.4	106.3	1.8	117.6	38.2/39.1
D	0.1049	1.8080	0.0160	0.1980	0.6360	102.1	0.4	101.3	3.5	80.6	78.3/82.2
E	0.1046	2.9410	0.0157	0.2350	0.5813	100.4	0.5	101.0	5.7	116.1	127.5/138.2
TB022 Revenue											
A	0.1098	0.3520	0.0165	0.1300	0.5438	105.5	0.3	105.8	0.7	113.2	14.2/14.3
B	0.7554	0.1460	0.0574	0.1070	0.6663	360.1	0.8	571.4	1.3	1535.6	4.1/4.1
C	0.5838	0.1640	0.0531	0.0980	0.6961	333.8	0.6	466.9	1.2	1189.1	4.7/4.7
D	0.1098	0.3180	0.0165	0.1110	0.5499	105.4	0.2	105.7	0.6	112.7	12.9/12.9
E	0.1095	0.5030	0.0165	0.2690	0.6666	105.5	0.6	105.5	1.0	104.4	17.9/18.1
TB174 Revenue											
A	0.1077	0.2050	0.0161	0.0940	0.6889	103.2	0.2	103.9	0.4	119.3	7.3/7.4
B	0.1085	0.2060	0.0163	0.1240	0.7131	104.5	0.3	104.6	0.4	106.2	6.9/6.9
C	0.1182	0.2290	0.0174	0.1680	0.7988	111.4	0.4	113.4	0.5	156.0	6.5/6.5
D	0.1085	0.2170	0.0164	0.1200	0.6932	104.6	0.3	104.6	0.4	104.2	7.5/7.6
E	0.1082	0.1810	0.0163	0.0900	0.7277	104.4	0.2	104.4	0.4	102.9	6.2/6.2
TB181 Revenue											
A	0.0756	0.4180	0.0116	0.0770	0.4999	74.2	0.1	74.1	0.6	69.2	18.3/18.5
B	0.0768	3.3320	0.0117	0.2960	0.6417	75.1	0.4	75.1	4.8	75.5	143.3/156.9
C	0.2041	0.1610	0.0280	0.1110	0.7951	178.3	0.4	188.6	0.6	319.6	4.5/4.5
D	0.0770	0.4070	0.0117	0.1740	0.4770	75.2	0.3	75.3	0.6	79.6	16.9/17.1

Note: A, B etc. are labels for fractions composed of single zircon grains or fragments.

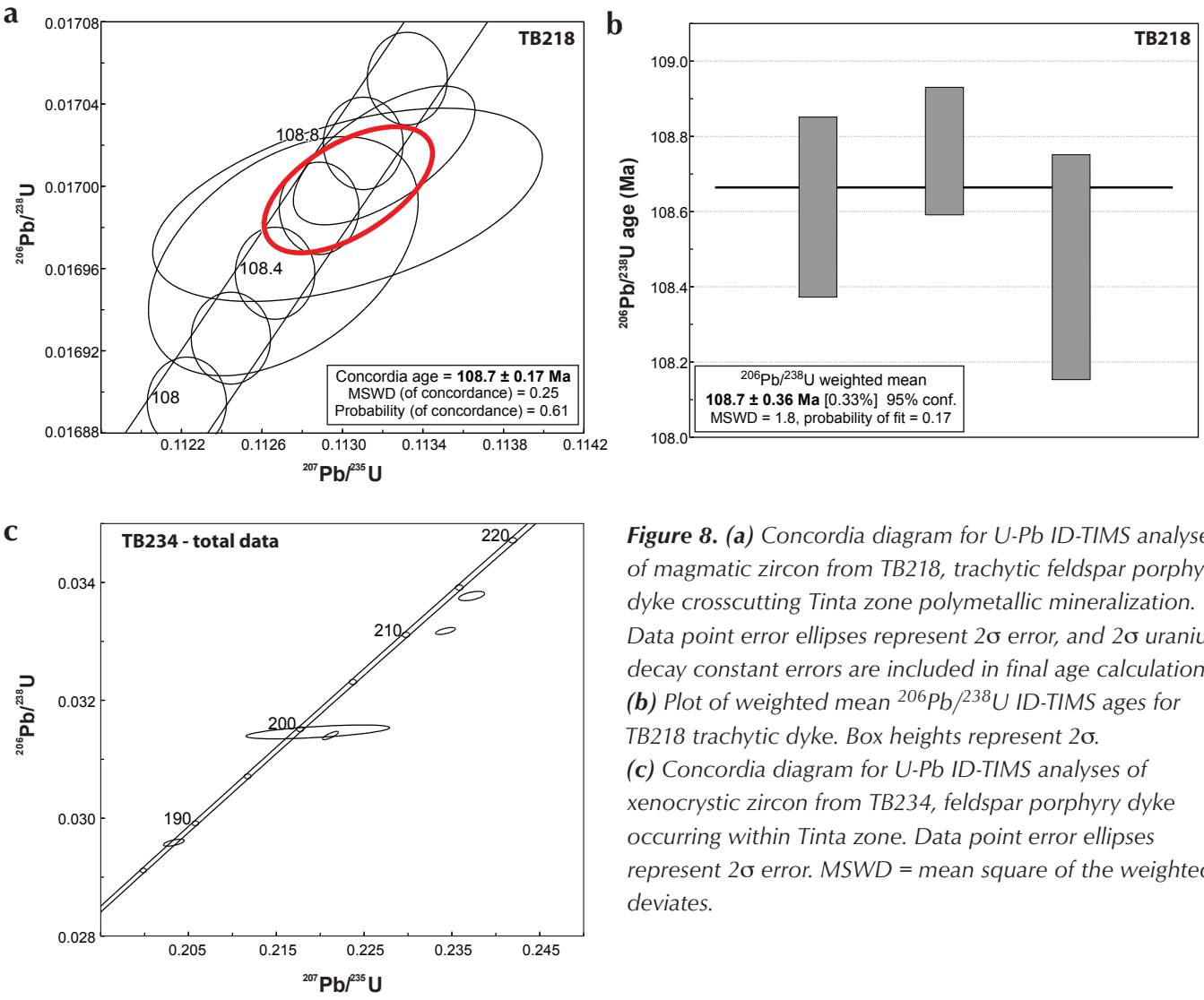

Figure 8. ***(a)*** *Concordia diagram for U-Pb ID-TIMS analyses of magmatic zircon from TB218, trachytic feldspar porphyry dyke crosscutting Tinta zone polymetallic mineralization. Data point error ellipses represent 2σ error, and 2σ uranium-decay constant errors are included in final age calculation.* ***(b)*** *Plot of weighted mean $^{206}Pb/^{238}U$ ID-TIMS ages for TB218 trachytic dyke. Box heights represent 2σ.* ***(c)*** *Concordia diagram for U-Pb ID-TIMS analyses of xenocrystic zircon from TB234, feldspar porphyry dyke occurring within Tinta zone. Data point error ellipses represent 2σ error. MSWD = mean square of the weighted deviates.*

with (i) destruction of primary plutonic textures in the monzodiorite, and (ii) local pyrite ± chalcopyrite mineralization hosted in the alteration selvedge. Five single-grain zircon fractions were analysed from TB022 (Table 2). Of the five fractions, three resulted in overlapping concordant analyses from which a concordia age of 105.5 ± 0.20 Ma and a weighted mean $^{206}Pb/^{238}U$ age of 105.5 ± 0.16 Ma were calculated (Fig. 9a and b). The two remaining fractions resulted in strongly discordant data, interpreted as inherited (Table 2).

Sample TB174 is a yellowish brown to pink feldspar porphyry dyke of trachydacitic composition that intrudes a strongly altered plutonic rock in Revenue zone (382613E, 6913285N). The dyke is strongly mineralized (chalcopyrite-pyrite-malachite-manganese oxides). Five single-grain zircon fractions were analysed from TB174 (Table 2). Of the five fractions, three resulted in overlapping concordant analyses from which a concordia age of 104.5 ± 0.17 Ma and a weighted mean $^{206}Pb/^{238}U$ age of 104.5 ± 0.13 Ma were calculated (Fig. 9c and d). The two remaining fractions resulted in discordant data and were not used in the age calculation (Table 2).

Sample TB183 (382690E 6912989N) is a fine-grained, equigranular monzonitic dyke comprised of predominantly feldspar, subordinate quartz (<10%) and rare biotite. Where sampled, the dyke intrudes a coarse-grained granitic pluton of similar mineralogy. Five single-grain zircon fractions were analysed from TB183 (Table 2). Of the five fractions, three resulted in overlapping concordant analyses from which a concordia age of 105.7 ± 0.22 Ma and a weighted mean $^{206}Pb/^{238}U$ age of 105.7 ± 0.19 Ma were calculated (Fig. 9e and f). The two remaining fractions also resulted in concordant data at

ca. 102 and 100 Ma, and are interpreted to be reset ages due to overprinting thermal events (Table 2).

Sample TB181 is a purple porphyritic dyke of rhyolitic composition and is comprised of distinctive 'quartz-eye' and feldspar phenocrysts hosted in an aphanitic, quartz-dominant groundmass. The dyke is weak to moderately sericite-saussurite-altered, and additionally, has notable malachite staining at the margins of the dyke when in contact with the country rock, which is an altered granitoid of unknown composition. Four single-grain zircon fractions were analysed from TB181 (Table 2). Of the four fractions, two resulted in overlapping concordant analyses from which a concordia age of 75.15 ± 0.23 Ma and a weighted mean $^{206}Pb/^{238}U$ age of 75.16 ± 0.22 Ma were calculated (Fig. 9g and h). The two remaining fractions also resulted in one strongly discordant older analysis interpreted as inherited, and one concordant

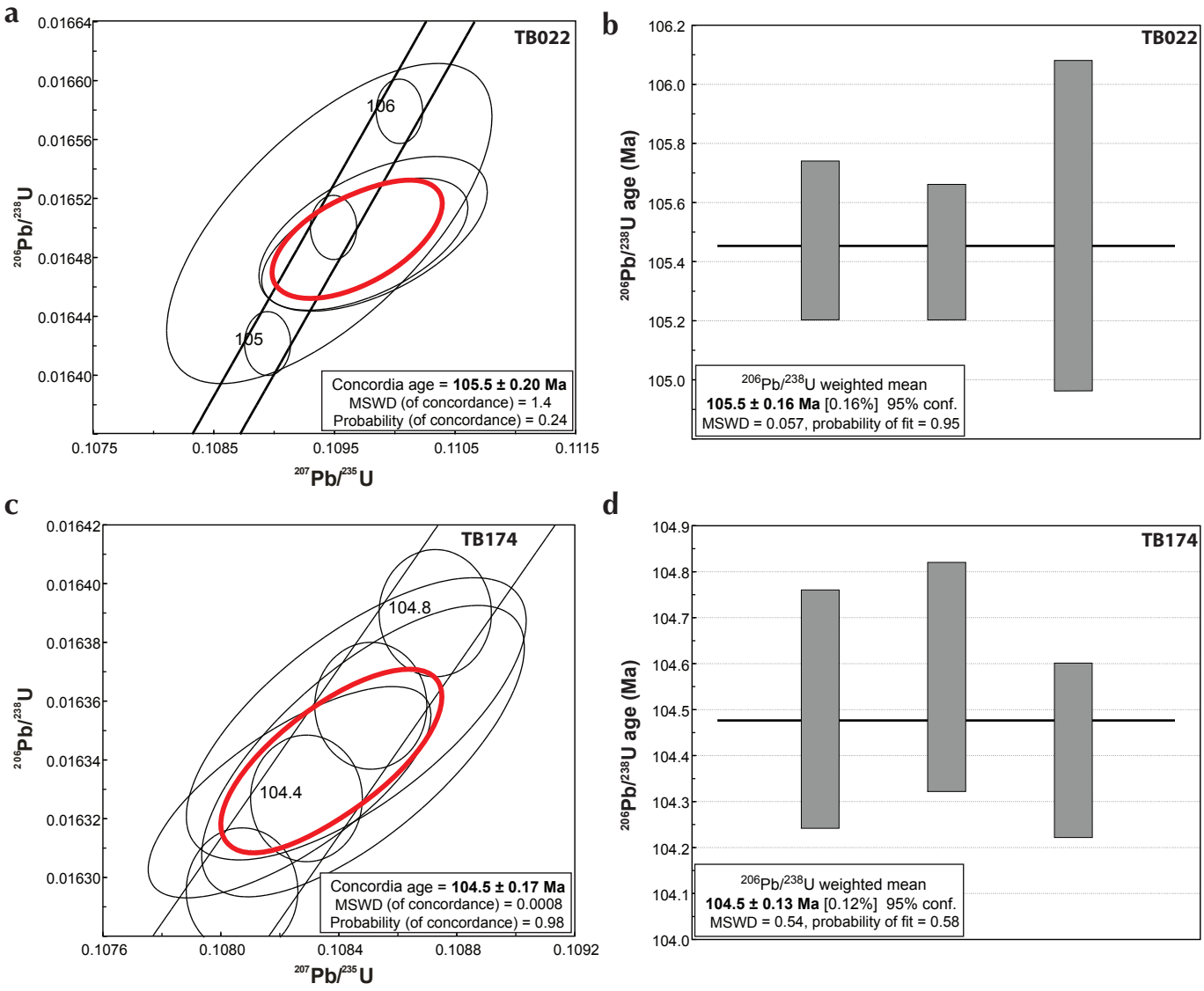

Figure 9. ***(a)*** *Concordia diagram for U-Pb ID-TIMS analyses of magmatic zircon from TB022; silicified feldspar porphyry dyke crosscutting Revenue Creek monzodiorite, Revenue zone. Data point error ellipses represent 2σ error, and 2σ uranium-decay constant errors are included in final age calculation.* ***(b)*** *Plot of weighted mean $^{206}Pb/^{238}U$ ID-TIMS ages for TB022; feldspar porphyry dyke, Revenue zone. Box heights represent 2σ.* ***(c)*** *Concordia diagram for U-Pb ID-TIMS analyses of magmatic zircon from TB174; feldspar porphyry dyke, Revenue zone.* ***(d)*** *Plot of weighted mean $^{206}Pb/^{238}U$ ID-TIMS ages for TB174; feldspar porphyry dyke, Revenue zone. Box heights represent 2σ. MSWD = mean square of the weighted deviates.* *(Figure 9e,f,g,h continued on next page.)*

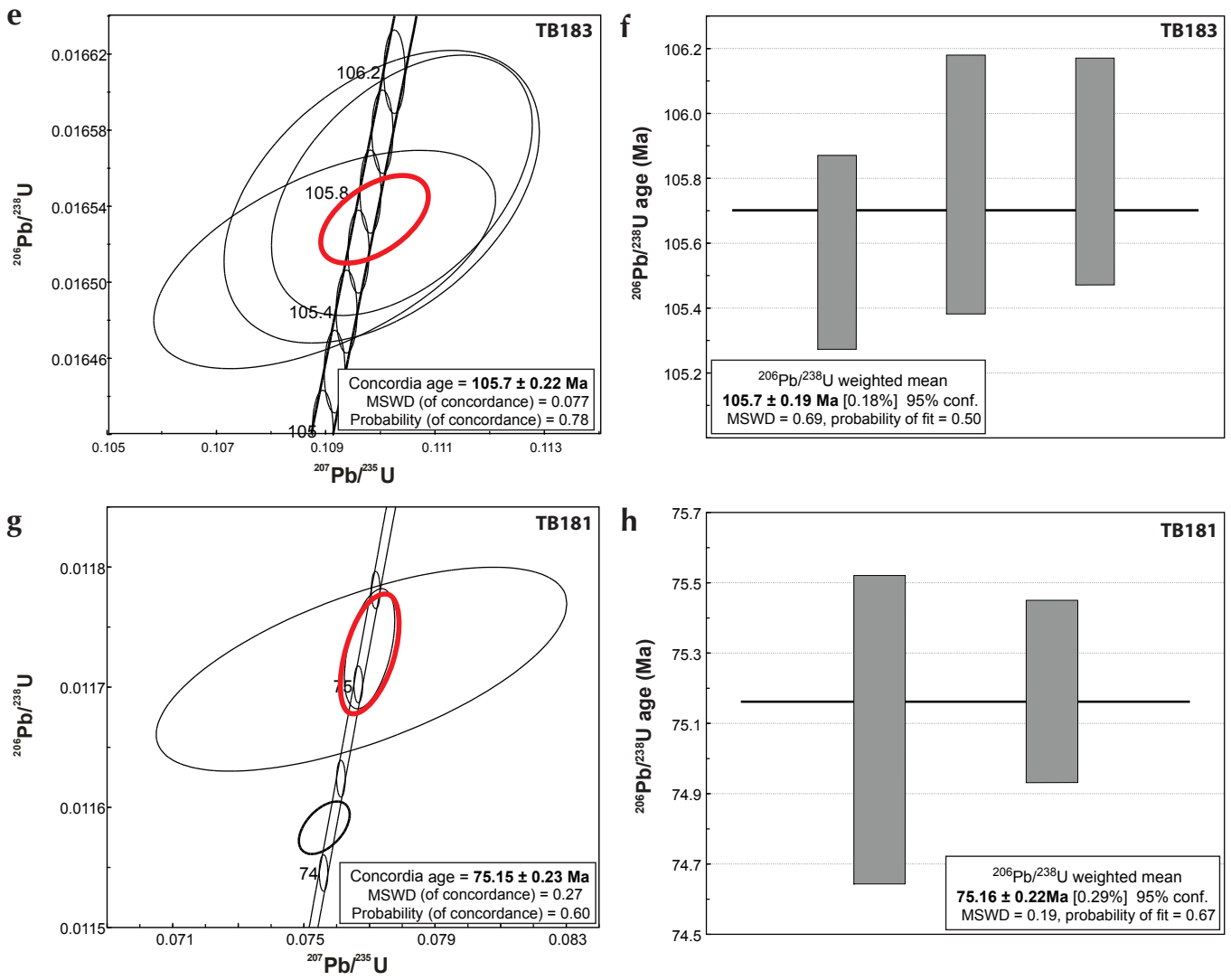

Figure 9. *continued (**e**) Concordia diagram for U-Pb ID-TIMS analyses of magmatic zircon from TB183; feldspar porphyry dyke, Revenue zone. Data point error ellipses represent 2σ error, and 2σ uranium-decay constant errors are included in final age calculation. **(f)** Plot of weighted mean $^{206}Pb/^{238}U$ ID-TIMS ages for TB183; feldspar porphyry dyke, Revenue zone. Box heights represent 2σ. **(g)** Concordia diagram for U-Pb ID-TIMS analyses of magmatic zircon from TB181; rhyolite dyke, Revenue zone. Data point error ellipses represent 2σ error, and 2σ uranium-decay constant errors are included in final age calculation. **(h)** Plot of weighted mean $^{206}Pb/^{238}U$ ID-TIMS ages for TB181; rhyolite dyke, Revenue zone. Box heights represent 2σ. MSWD = mean square of the weighted deviates.*

analysis at *ca.* 74 Ma, which is interpreted as resetting ages (Table 2).

A sample of the Revenue Creek monzodiorite was collected at the feldspar porphyry dyke U-Pb locality (sample TB022; Fig. 10) in order to better constrain the age of plutonism into which the Revenue feldspar dykes intrude. The site relationships are described above and illustrated in Figure 10c.

Abundant zircon of moderate quality was extracted from the sample of the Revenue Creek monzodiorite. Two morphologically distinct populations are present in subequal amounts: (i) clear, well-faceted equidimensional prisms (Fig. 11a), and (ii) elongate to irregular prisms with core and rim zircon growth (Fig. 11b). BSE and CL imaging of both zircon populations demonstrates that magmatic zircon occurs as both entire grains and as thick magmatic

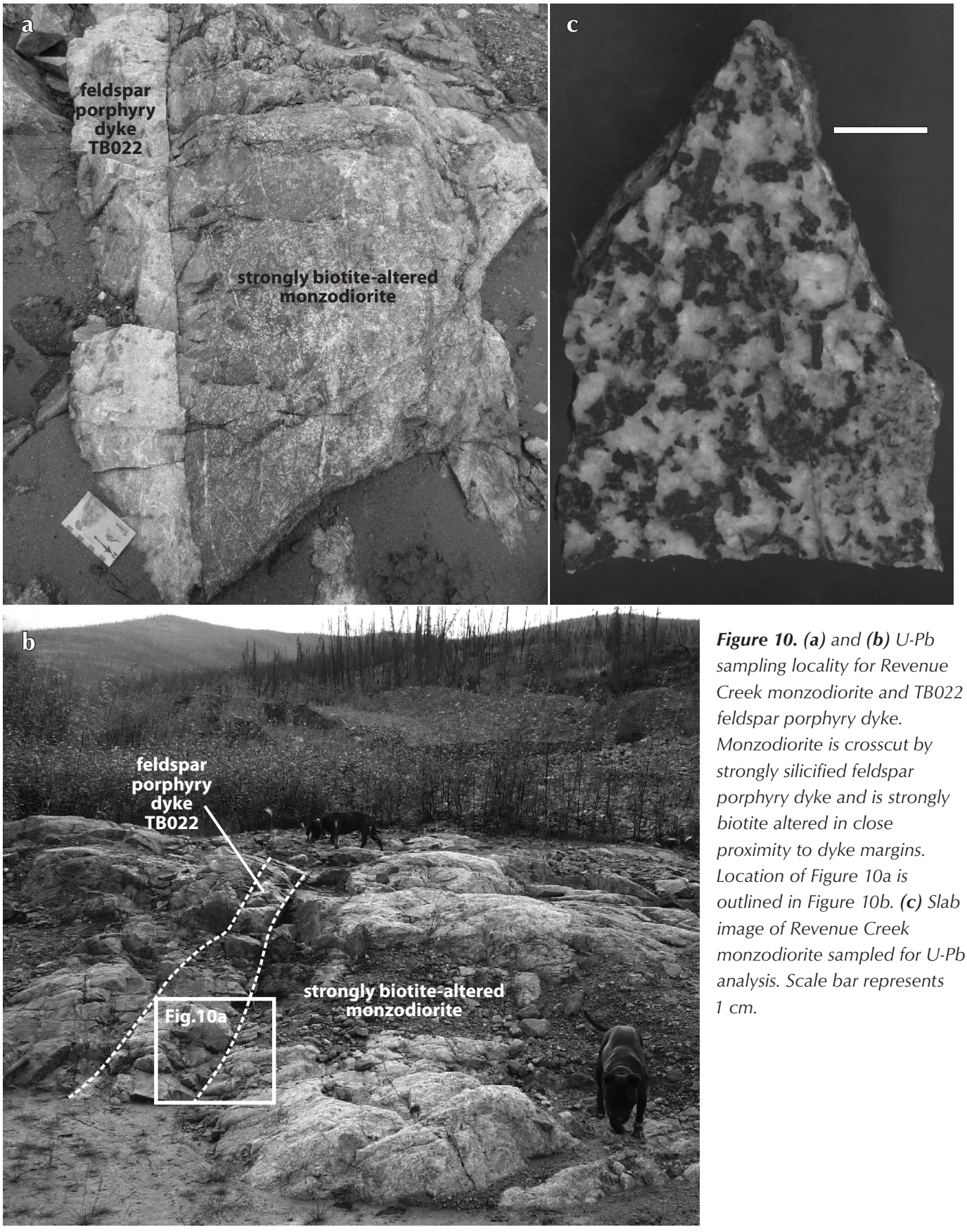

Figure 10. ***(a)*** *and* ***(b)*** *U-Pb sampling locality for Revenue Creek monzodiorite and TB022 feldspar porphyry dyke. Monzodiorite is crosscut by strongly silicified feldspar porphyry dyke and is strongly biotite altered in close proximity to dyke margins. Location of Figure 10a is outlined in Figure 10b.* ***(c)*** *Slab image of Revenue Creek monzodiorite sampled for U-Pb analysis. Scale bar represents 1 cm.*

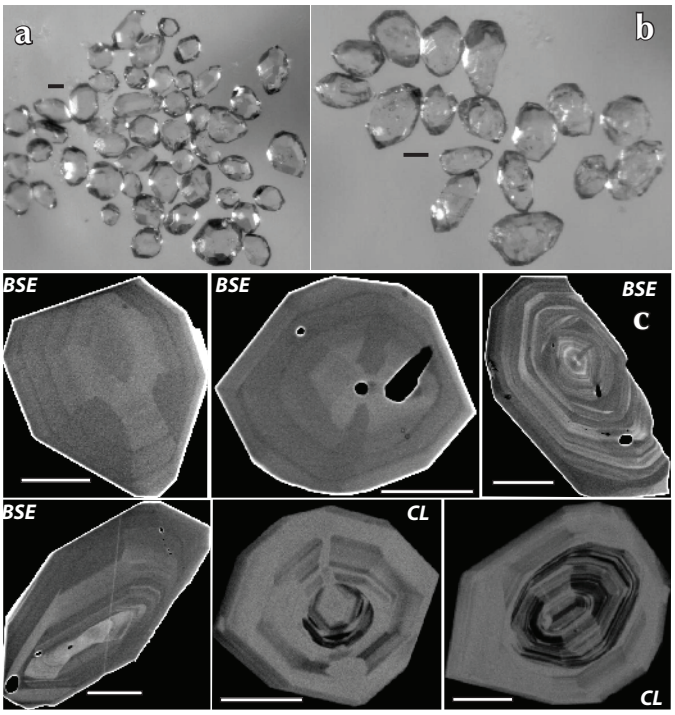

Figure 11. *Transmitted light images of* ***(a)*** *stubby, equidimensional zircon prism population, and* ***(b)*** *overgrowth population of zircons from Revenue Creek monzodiorite. Scale bars represent 50 mm.* ***(c)*** *BSE and CL images (denoted on image) of magmatic zircon occurring as entire grains and magmatic overgrowths on xenocrystic cores (CL images). Scale bars represent 50 μm. BSE = backscattered electron, CL = cathodoluminescence.*

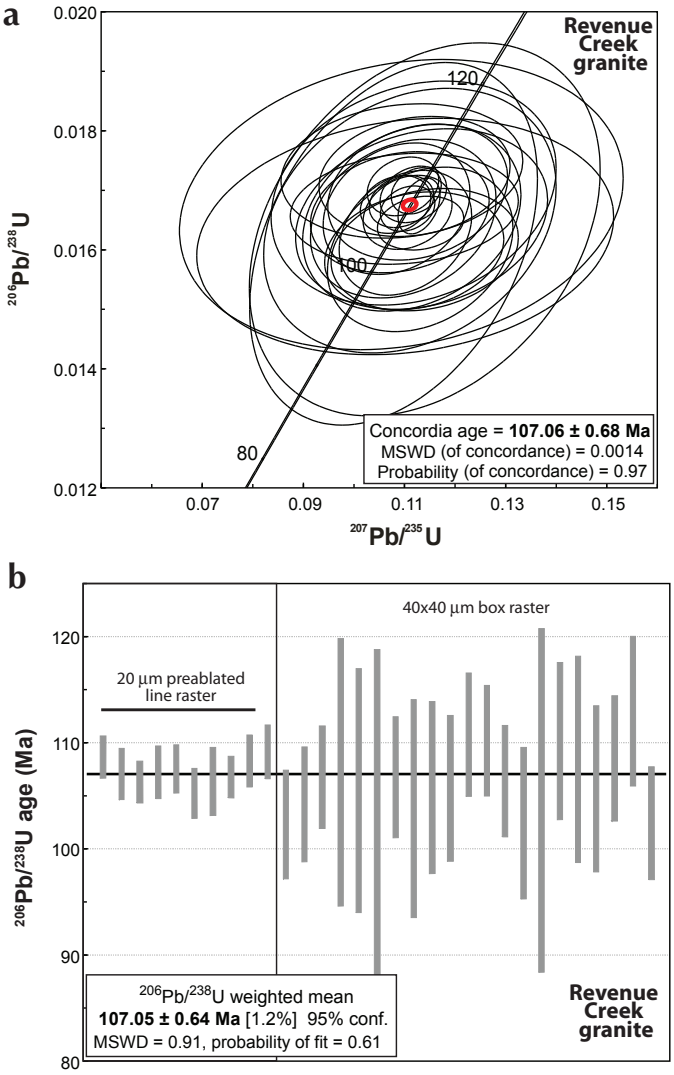

Figure 12. ***(a)*** *Concordia diagram for U-Pb LAM ICP-MS analyses of magmatic zircon from Revenue Creek monzodiorite. Individual analyses with probability of concordance less than 0.2 are not included in final data calculations. Data point error ellipses represent 2σ error, and 2σ uranium-decay constant errors are included in final age calculation.* ***(b)*** *Plot of weighted mean $^{206}Pb/^{238}U$ ages with probability of concordance greater than 0.20. Box heights represent 2σ. MSWD = mean square of the weighted deviates.*

rims, and that magmatic zircon is characterized by more diffuse oscillatory zoning (Fig. 11c).

Thirty-one analyses were collected from both magmatic zircon grains and magmatic rims (Appendix 1). Twenty micron-diameter line rasters were employed to analyze zircon rims, whereas 40 x 40 μm box rasters were used to analyze magmatic zircon grains. A concordia age calculated from 31 analyses yielded an age of 107.06 ± 0.68 Ma (MSWD = 0.0014) and a weighted mean $^{206}Pb/^{238}U$ age of 107.05 ± 0.649 Ma (MSWD = 0.91; Fig. 12a and b). Concentration data calculated from magmatic zircon varies from 128 ppm to 729 ppm U, and 54 ppm to 301 ppm Th (Appendix 1).

STODDART ZONE

Two intrusive rocks were sampled from the Stoddart zone including an aplitic dyke (TB369) and a porphyritic andesitic dyke (TB038). Both dykes are observed to crosscut the Stoddart granite. The aplitic dyke was dated using ID-TIMS, whilst U-Pb dating of the andesitic dyke was done using LAM ICP-MS.

Sample TB369 is one of a suite of aplitic dykes that crosscut the Stoddart porphyry. Additionally, the aplite dykes are observed to be overprinted by quartz-chalcopyrite-molybdenite ± scheelite mineralized veins for which the molydenite has a Re-Os age of *ca.* 94 Ma (Fig. 6c). Four single-grain zircon fractions were analysed from TB369 (Appendix 2) and four concordant analyses of widely different ages (*ca.* 162 Ma, 102 Ma, 97 Ma and 78 Ma; Fig. 13a) were obtained. The spread in concordant U-Pb age data can only be interpreted by taking into consideration the age of molybdenite mineralization at Stoddart (*ca.* 94 Ma) and the age of TB038 (*ca.* 77 Ma, outlined below). The fractions yielding concordant ages of *ca.* 162 Ma and 102 Ma are considered to represent inheritance. The concordant analysis yielding an age of *ca.* 78 Ma is consistent with the age of crystallization of TB038 and is thus interpreted as a reset age. If the age of molybdenite mineralization is constrained to *ca.* 94 Ma, then the third fraction, which has a concordia age of 97.9 ± 0.40 Ma (Fig. 13b), is considered the best estimate of the crystallization age of the aplitic dyke and is consistent with the overprinting chalcopyrite-molybdenite ± scheelite mineralized veins observed in core.

TB038 was sampled from the Stoddart zone where a weakly mineralized porphyritic andesitic dyke crosscuts an equigranular phase of the Stoddart granitic intrusion (Fig. 14). The andesite dyke consists of coarse-grained plagioclase, hornblende, biotite and quartz phenocrysts with weak to moderate flow alignment in a fine-grained groundmass of similar mineralogy. Malachite staining was observed at the margins of the andesitic dyke, similar to that observed for TB181 within the Revenue zone.

The sample yielded abundant zircons of moderate to good quality, from which three morphologically distinct populations could be recognized, including: (i) elongate to irregular prisms with core and rim zircon growth (Fig. 15a), (ii) clear, well-faceted equidimensional prisms (Fig. 15b), and (iii) elongate prisms transitional to needle-shaped populations (Fig. 15c). BSE and CL imaging of the zircon populations demonstrates that magmatic zircon occurs as both entire grains and as magmatic rims and that the magmatic zircon is characterized by more diffuse to sharp oscillatory zoning (Fig. 15d).

Twenty-six analyses were collected from both magmatic zircon grains and magmatic rims (Appendix 3). A concordia age calculated from 22 analyses yielded an age of 76.86 ± 0.86 Ma (MSWD = 0.0023) and a weighted mean $^{206}Pb/^{238}U$ age of 76.89 ± 0.86 Ma (MSWD = 0.57; Fig. 16a and b). Concentration data calculated from

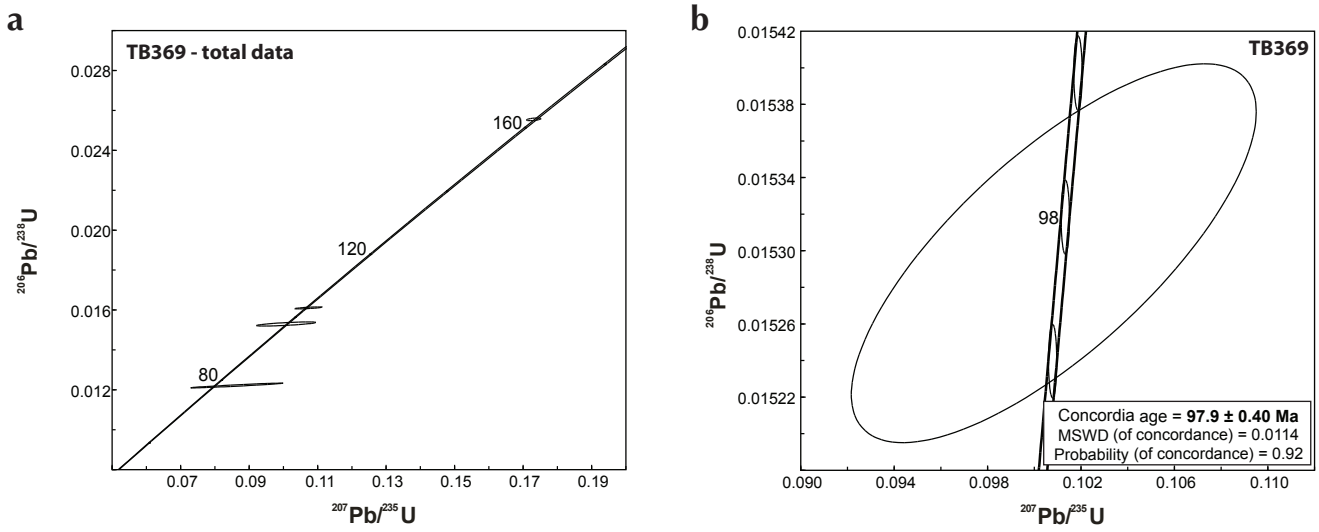

Figure 13. (a) *Concordia diagram for U-Pb ID-TIMS analyses of magmatic zircon from TB369; aplitic dyke crosscutting Stoddart zone Cu-Mo-W mineralization.* ***(b)*** *Plot of weighted mean $^{206}Pb/^{238}U$ ID-TIMS ages for TB369; aplitic dyke crosscutting Stoddart zone granite. Box heights represent 2σ. MSWD = mean square of the weighted deviates.*

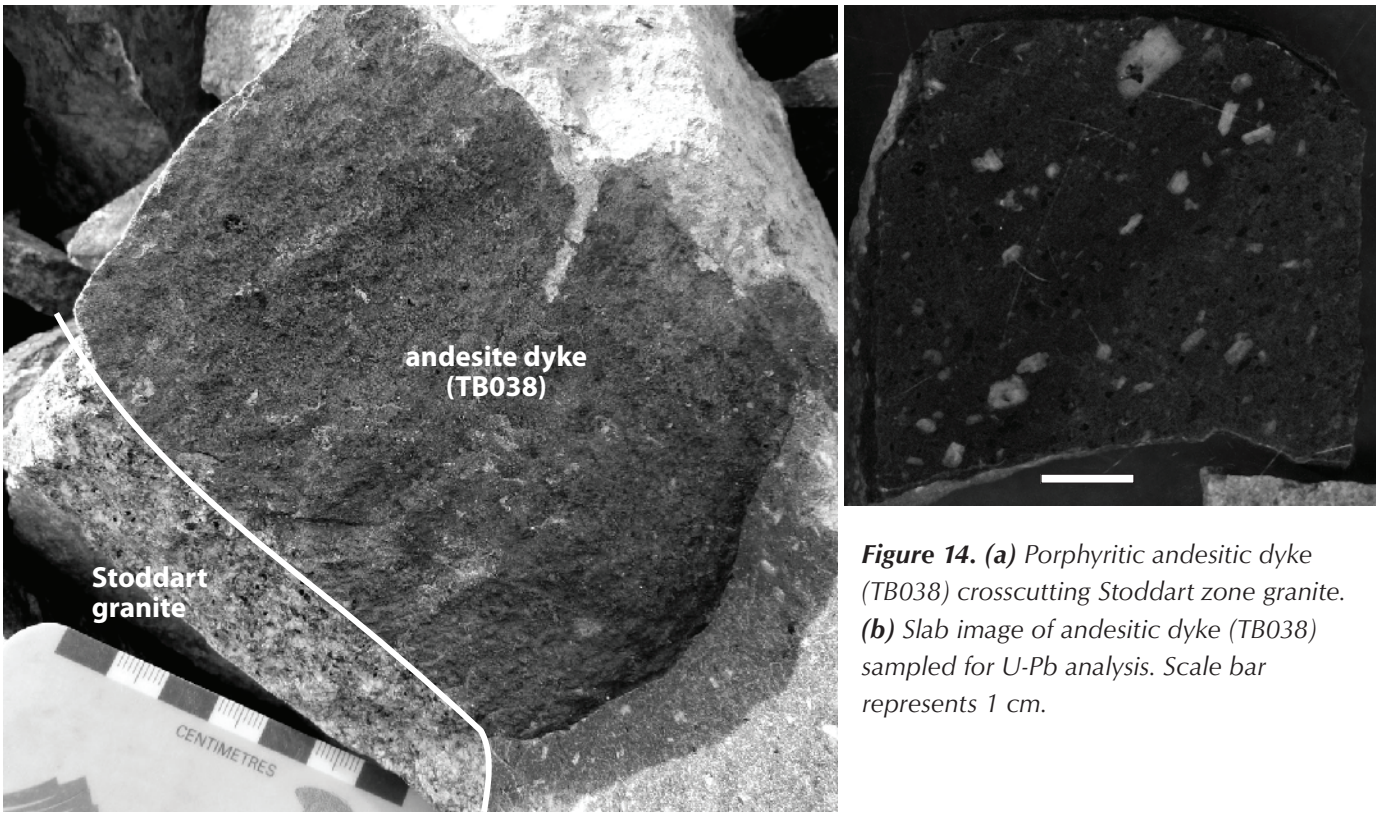

Figure 14. *(**a**) Porphyritic andesitic dyke (TB038) crosscutting Stoddart zone granite. (**b**) Slab image of andesitic dyke (TB038) sampled for U-Pb analysis. Scale bar represents 1 cm.*

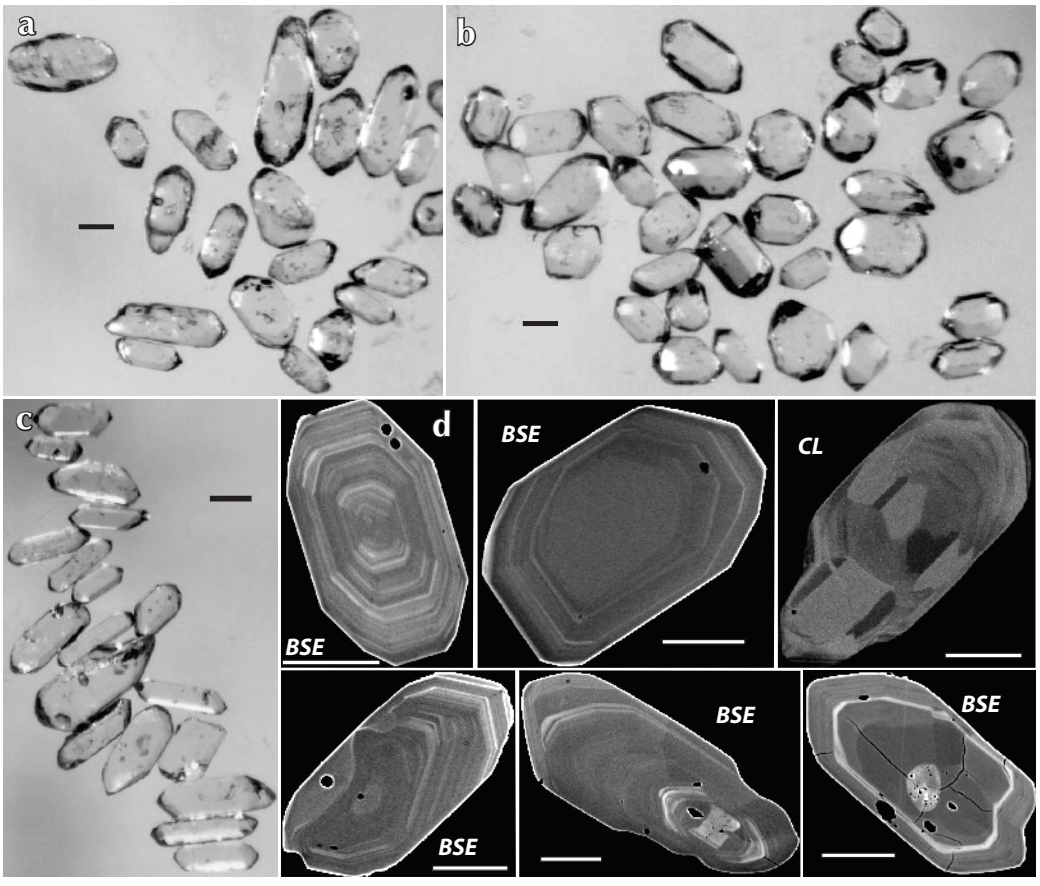

Figure 15. *Transmitted light images of **(a)** overgrowth zircon population, **(b)** well-faceted, stubby zircon prism population, and **(c)** zircon needle and elongate prism population (with some overgrowth tips) of zircons from andesitic dyke (TB038). Scale bars represent 50 mm. **(d)** BSE and CL images (denoted on image) of magmatic zircon from andesitic dyke (TB038) occurring as entire grains and magmatic overgrowths on xenocrystic cores. All scale bars represent 50 μm. BSE = backscattered electron, CL = cathodoluminescence.*

magmatic zircon varies from 105 ppm to 2118 ppm U, and 44 ppm to 1588 ppm Th (Appendix 3).

RIDGE ZONE

Observations from the Ridge zone trench and drill core indicate that mineralization in this zone postdates the intrusion of the Bow Creek granite (Fig. 17a). A sample of the Bow Creek granite from the Ridge zone mineralized trench was collected to place a maximum age constraint on the timing of mineralization associated with dolomitic alteration within this zone (Fig. 17b and c).

The sample yielded abundant zircon of good quality from which three morphologically distinct populations could be recognized, including: (i) translucent, well-faceted, equidimensional prisms (Fig. 18a), (ii) elongate to irregular prisms with core and rim zircon growth (Fig. 18b), and (iii) subordinate, large needle and needle fragment population (Fig. 18c). BSE and CL imaging of the zircon populations demonstrates magmatic zircon occurs as entire grains and as magmatic rims, and that magmatic zircon is characterized by diffuse to sharp oscillatory and sector zoning (Fig. 18d).

Thirty analyses were collected from both magmatic zircon grains and magmatic rims (Appendix 4). A concordia age calculated from 23 analyses yielded an age of 68.25 ± 0.90 Ma (MSWD = 1.6) and a weighted mean $^{206}Pb/^{238}U$ age of 68.43 ± 0.91 Ma (MSWD = 0.37; Fig. 19a and b). Concentration data calculated from magmatic zircon varies from 148 ppm to 1380 ppm U, and 37 ppm to 1057 ppm Th (Appendix 4).

DISCUSSION AND CONCLUSIONS

The NFR Freegold Mountain project is host to several discrete mineralized zones, including two with NI 43-101 resources, *e.g.*, the Tinta Deposit (Au-Ag-Cu-Pb-Zn) and the Nucleus (Au) Deposit. Each mineralized zone is associated with a different metal suite of interest and corresponding style and setting of mineralization indicative of a tectonic setting involving a complex interplay of long-lived structural conduits and multiphase fertile magmatism.

Quartz-feldspar porphyry dyke relationships within the Tinta zone indicate that structurally controlled, polymetallic mineralization took place prior to 108.7 ± 0.4 Ma (zircon). A U-Pb age from hornblende-biotite monzodiorite, which is crosscut by Nucleus-style Au-Cu mineralized dykes in Revenue Creek

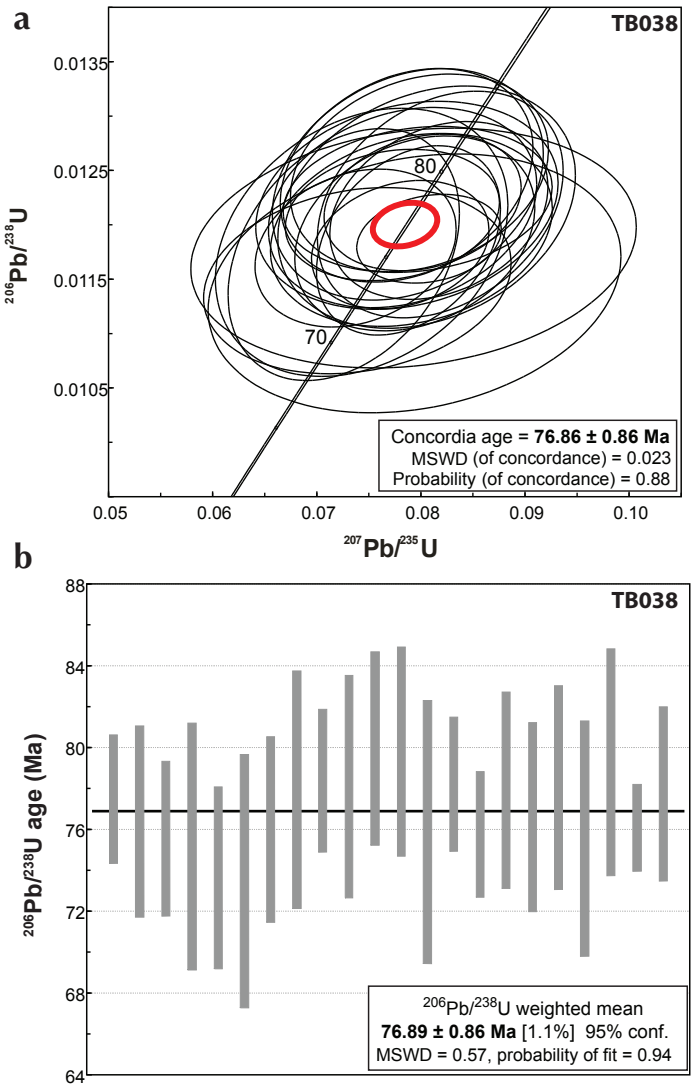

Figure 16. (a) *Concordia diagram for U-Pb LAM ICP-MS analyses of magmatic zircon from andesitic dyke, TB038. Individual analyses with probability of concordance less than 0.2 are not included in final data calculations. Data point error ellipses represent 2σ error, and 2σ uranium-decay constant errors are included in final age calculation.* ***(b)*** *Plot of weighted mean $^{206}Pb/^{238}U$ ages with probability of concordance greater than 0.20 for magmatic zircon from andesitic dyke, TB038. Box heights represent 2σ. MSWD = mean square of the weighted deviates.*

Figure 17. ***(a)*** *Core photo of epithermal dolomite vein crosscutting Bow Creek granite, Ridge zone. Location of 17b marked.* ***(b)*** *Rotated enlargement of dolomite vein exhibiting epithermal veining textures.* ***(c)*** *Slab image of Bow Creek granite sampled from Ridge zone for U-Pb analysis. Scale bars represent 1 cm.*

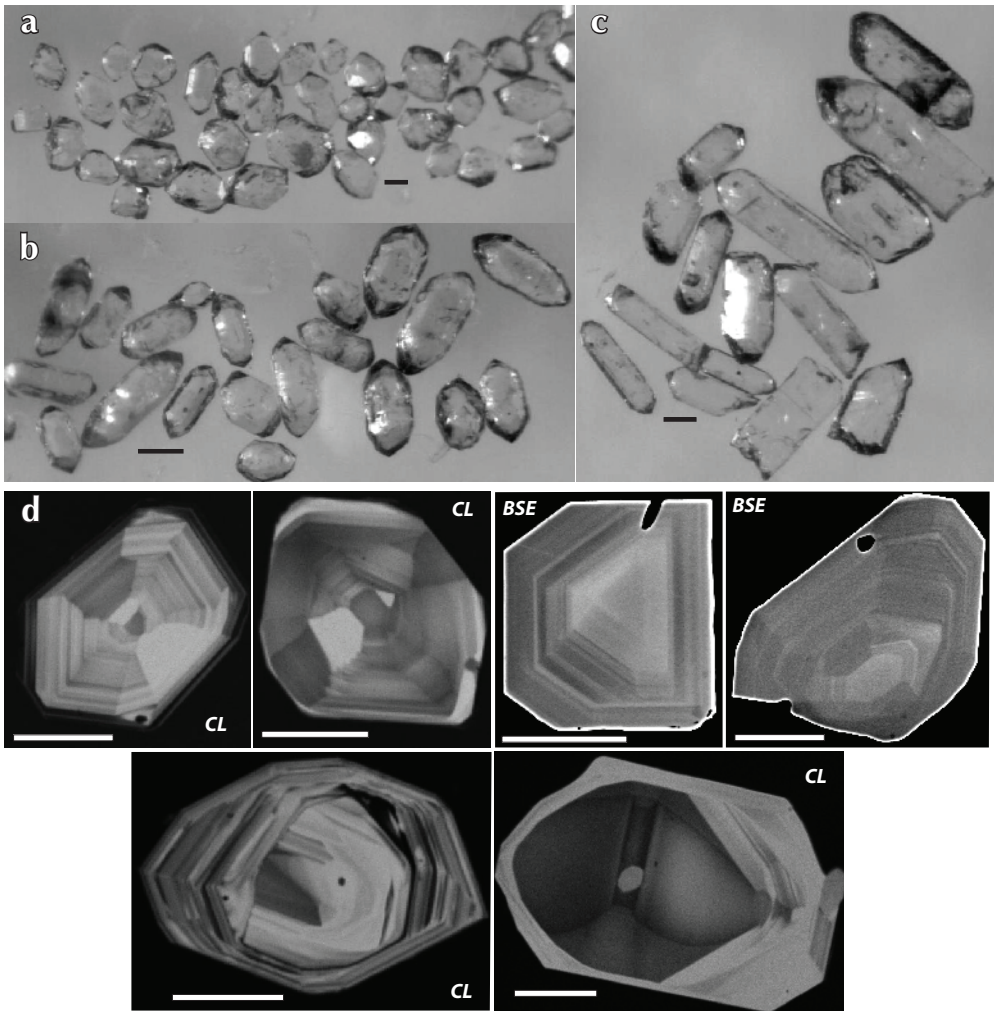

Figure 18. *Transmitted light images of* ***(a)*** *well-faceted, equidimensional zircon prism population,* ***(b)*** *overgrowth population, and* ***(c)*** *zircon needle population (with some overgrowth tips) from Bow Creek granite. Scale bars represent 50 mm.* ***(d)*** *BSE and CL images (denoted on image) of magmatic zircon from Bow Creek granite. All scale bars represent 50 μm.*
BSE = backscattered electron, CL = cathodoluminescence.

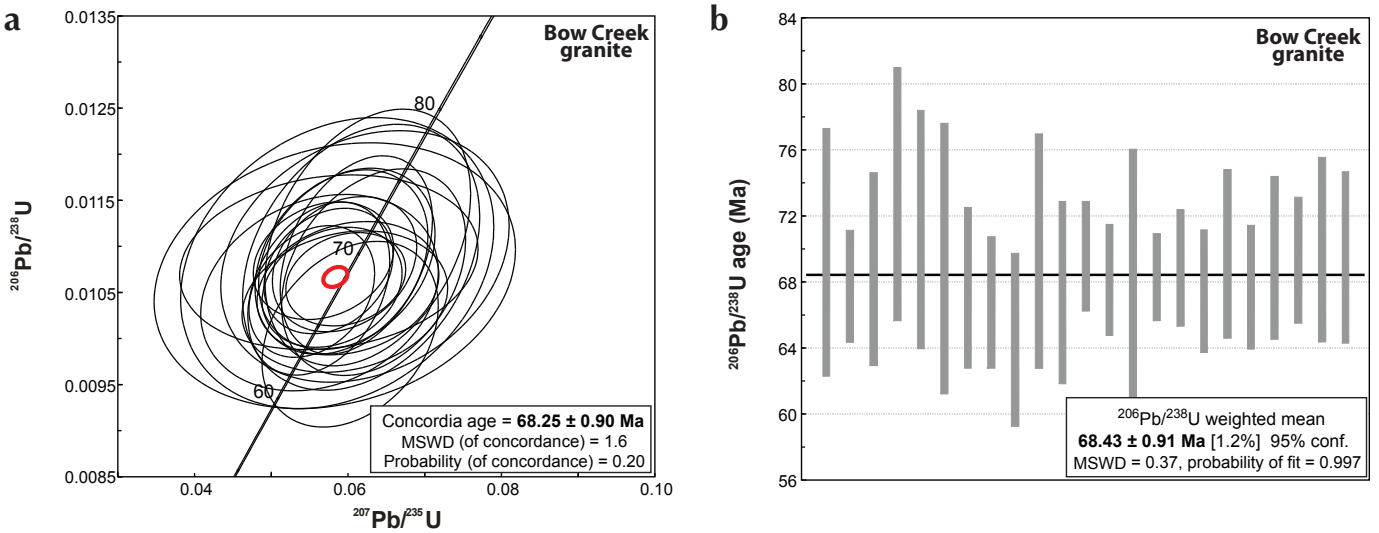

Figure 19. ***(a)*** *Concordia diagram for U-Pb LAM ICP-MS analyses, Bow Creek granite. Individual analyses with probability of concordance less than 0.2 are not included in final data calculations. Data point error ellipses represent 2σ error, and 2σ uranium-decay constant errors are included in final age calculation.* ***(b)*** *Plot of weighted mean $^{206}Pb/^{238}U$ ages with probability of concordance greater than 0.20 for magmatic zircon from Bow Creek granite. Box heights represent 2σ. MSWD = mean square of the weighted deviates.*

(105.7 ± 0.2 Ma, 105.5 ± 0.2 Ma and 104.4 ± 0.1 Ma; U-Pb zircon), yields an age of 107.1 ± 0.6 Ma (U-Pb zircon), demonstrating a broadly synchronous relationship. The Stoddart Cu-Mo-W porphyry is crosscut by several dyke suites ranging from aplitic to andesitic and basaltic in composition. A U-Pb zircon age from an aplitic dyke that crosscuts the Stoddart porphyry, but is itself crosscut by Cu-Mo-W vein mineralization, yields an age of 97.9 ± 0.4 Ma, consistent with the younger Re-Os molybdenite model age of 93.7 ± 1.5 Ma. An andesitic dyke that locally hosts Cu mineralization, and which crosscuts the Stoddart biotite granite, yielded an age of 76.9 ± 0.9 Ma (U-Pb zircon). This age and style of mineralization has also been recorded from a rhyolitic dyke that intrudes the Revenue zone (75.2 ± 0.2 Ma; U-Pb zircon). Shear-hosted, polymetallic Au-Ag-Pb-Cu mineralization occurring at the Ridge zone, which occurs at or near the contact between the Casino granodiorite and the Bow Creek granite, is characterized by both base-metal-bearing silica and dolomitic fluids. Importantly, galena-rich dolomitic veins are observed to crosscut the Bow Creek granite, which yielded a U-Pb zircon date of 68.4 ± 0.9 Ma, indicating that dolomitic fluids associated with the Ridge zone post date the intrusion of the Bow Creek granite.

Collectively, the new age data determined from Cretaceous magmatic units that intrude the Tinta, Revenue, Stoddart and Ridge mineralized zones demonstrate that a protracted history of economically important, polymetallic mineralization extended for more than 40 Ma (Fig. 20). Importantly, these new age data place maximum and minimum age constraints on the timing of mineralization occurring across the Freegold Mountain project area.

	Age (Ma)	Magmatic event	Mineralization event
Late Cretaceous	Post 68 Ma	Ridge zone polymetallic mineralization, base-metal mineralization associated with epithermal dolomite veins crosscuts Bow Creek granite	Ridge zone (polymetalllic)
	68 Ma (U-Pb)	Intrusion of Bow Creek granite	
	75 Ma (U-Pb)	Rhyolitic Revenue dyke emplacement	Revenue late-stage Cu-Au
	77 Ma (U-Pb)	Andesitic dyke crosscutting Stoddart zone granite	
Mid Cretaceous	~94 Ma (Re-Os)	Cu-Mo-W mineralization, Stoddart porphyry	Stoddart zone (Cu-Mo-W)
	~98 Ma (U-Pb)	Intrusion of aplite dykes crosscutting Stoddart granite	
	106 - 104 Ma (U-Pb)	Intrusion of Nucleus and Revenue dykes	Nucleus and Revenue (Au-Cu) skarn and later dyke and structurally hosted Au-Cu mineralization
	107 Ma (U-Pb)	Intrusion of Revenue Creek granite	
	Pre 109 Ma	Chlorite-altered trachytic dyke crosscuts polymetallic mineralization, Tinta zone	
	Pre 109 Ma(?)	Tinta zone mineralization crosscutting Jurassic(?) granite	Tinta zone (polymetallic)

Figure 20. *Summary diagram illustrating the distribution through time of important magmatic and mineralizing events known to occur throughout the Freegold Mountain project area.*

ACKNOWLEDGEMENTS

We thank the Yukon Geological Survey (YGS), Northern Freegold Resources (NFR), and NSERC for funding and logistical support. We are also grateful to David Lentz from University of New Brunswick, for supervising the PhD thesis of Thierry Bineli Betsi and for pre-reviewing this manuscript. We acknowledge Fabrizio Colombo, Wade Barnes, Roger Hulstein and Emily Miller, all from NFR, for their assistance during field work. Thank you to Pam King, Earth Sciences Department, Memorial University and Michael Tubrett and Michael Schaeffer for access and assistance in the MafIIC analytical facility. Grant Abbott provided clarity on terminology and the regional geology section. Roger Hulstein and Wade Barnes are thanked for comments on an earlier draft of the manuscript.

REFERENCES

Bennett, V. and Tubrett, M., 2010 (this volume). U-Pb isotopic age dating by LAM ICP-MS, INCO Innovation Centre, Memorial University: Sample preparation, methodology and analytical techniques. *In:* Yukon Exploration and Geology 2009, K.E. MacFarlane, L.H. Weston and L.R. Blackburn (eds.), Yukon Geological Survey, p. 47-55.

Carlson, G.G., 1987. Geology of Mount Nansen (115-1/3) and Stoddart Creek (115-1/6) map areas Dawson Range, Central Yukon. Exploration and Geological Services Division, Yukon Region, Indian and Northern Affairs Canada, Open File 1987-2, 181 p.

Colpron, M.N., Nelson, J.L. and Murphy, D.C., 2006. A tectonostratigraphic framework for the Pericratonic terranes of the northern Canadian Cordillera. *In*: Paleozoic evolution and metallogeny of Pericratonic Terrranes at the ancient pacific margin of North America, Canadian and Alaskan Cordillera. M. Colpron and J.L. Nelson (eds.), Geological Association of Canada, Special Paper 45, p. 1-23.

Crowley, J.L., Schoene B. and Bowring S.A., 2007. U-Pb dating of zircon in the Bishop Tuff at the millennial scale. Geology, vol. 35, p. 1123-1126.

Eaton, W.D., 1984. Geological , geochemical, and geophysical report for bulldozer trenching and diamond drilling program at Nat Joint Venture Nucleus 1-141 claims. Archer, Cathro & Associates, Assessment Report #091600.

Fonseca, A., 2009. NI 43-101 technical report on the Freegold Mountain property, Dawson Range, Yukon. <*http://www.sedar.com*>, 167 p., {Sept 9, 2009}.

Geospec Consultants Ltd., 2008. Re-Os isotopic analyses and age dating of Molybdenite for Northern Freegold Resources Ltd.

Gordey, S.P. and Makepeace, A.J. (comps.), 2000. Bedrock geology, Yukon Territory. Geological Survey of Canada, Open File 3754, and Exploration and Geological Services Division, Yukon Region, Indian and Northern Affairs Canada, Open File 2001-1, 1:1 000 000 scale.

Jaffey, A.H., Flynn, K.F., Glendenin, L.E., Bentley, W.C. and Essling, A.M., 1971. Precision measurements of half-lives and specific activities of ^{235}U and ^{238}U. Physical Review C, vol. 4, p. 1889-1906.

Johnston, S.T., 1995. Geological compilation with interpretation from geophysical surveys of the northern Dawson Range, central Yukon (115-J/9 and 115- J/10, 115-J/12, 1: 100 000-scale map). Exploration and Geological Services Division, Yukon Region, Indian and Northern Affairs Canada, Open File 1995-2 (G), 171 p.

Johnston, S.T., Mortensen, J.K. and Erdmer, P., 1996. Igneous and metaigneous age constraints for the Aishihik metamorphic suite, southwest Yukon. National Research Council of Canada, Canadian Journal of Earth Sciences, vol. 33, no. 11, p. 1543-1555.

Ludwig, K.R., 1999. User's manual for Isoplot/Ex, version 2.06: a geochronological toolkit for Microsoft Excel. Berkeley Geochronological Center, Special Publication No. 1a.

Mattinson, J.M., 2005. Zircon U-Pb chemical abrasion (CA – TIMS) method: combined annealing and multi-step dissolution analysis for improved precision and accuracy of zircon ages. Chemical Geology, vol. 220, p. 47-56.

McCausland, P.J.A., Symons, D.T.A., Hart, C.J.R. and Blackburn, W.H., 2001. Paleomagnetic study of the Late Cretaceous Seymour Creek stock, Yukon: Minimal geotectonic motion of the Yukon-Tanana Terrane, *In:* Yukon Exploration and Geology 2000, D.S. Emond and L.H. Weston (eds.), Exploration and Geological Services Division, Yukon Region, Indian and Northern Affairs Canada, p. 207-216.

Mortensen, J.K., Ghosh, D. and Ferri, F., 1995. U-Pb age constraints on intrusive rocks associated with copper-gold porphyry deposits in the Canadian Cordillera. *In*: Porphyry Deposits of the Northwestern Cordillera of North America, T.G. Schroeter (ed.), CIM Special Volume 46, p. 142-158.

Payne, J.G., Gonzalez, R.A., Akhurst, K. and Sisson W.G., 1987. Geology of Colorado Creek (115-J/10), Selwyn River (115-J/9), and Prospector Mountain (115-1/5) map areas, western Dawson Range, west-central Yukon. Exploration and Geological Services Division, Yukon Region, Indian and Northern Affairs Canada, Open File 1987-3, 141 p.

Schmitz, M.D. and B. Schoene, 2007. Derivation of isotope ratios, errors, and error correlations for U-Pb geochronology using ^{205}Pb-^{235}U-(^{233}U)-spiked isotope dilution thermal ionization mass spectrometric data. Geochemistry, Geophysics, Geosystems, vol. 8, Q08006, doi:10.1029/2006GC001492.

Selby, D., Creaser, R.A. and Nesbit, E.B., 1999. Major and trace element compositions and Sr-Nd-Pb systematics of crystalline rocks from the Dawson Range, Yukon, Canada. Canadian Journal of Earth Sciences, vol. 36, p. 1463-1481.

Tempelman-Kluit, D.J., 1974. Reconnaissance geology of Aishihik Lake, Snag and part of Stewart River map-areas, west-central Yukon (115A, 115F, 115G and 115K). Geological Survey of Canada, Paper 73-41, 97 p.

Tempelman-Kluit, D.J., 1984. Geology, Laberge (105E) and Carmacks (105I), Yukon Territory. Geological Survey of Canada, Open File 1101, maps with legends, 1:250 000 scale.

Appendix 1. *LAM ICP-MS U-Pb isotopic analyses of magmatic zircons from Revenue Creek granite.*

	Measured isotopic ratios							Calculated ages										
Analysis	$^{207}Pb/^{235}U$	1σ err.	$^{206}Pb/^{238}U$	1σ err.	Rho	$^{207}Pb/^{206}Pb$	1σ err.	$^{207}Pb/^{235}U$ Ma	1σ err. Ma	$^{206}Pb/^{238}U$ Ma	1σ err. Ma	Conc. age (Ma)	2σ err. Ma	MSWD of conc.	Prob. of conc.	Th (ppm)	U (ppm)	Ratio Th/U
oc19c15	0.1123	0.0020	0.0170	0.0002	0.2591	0.0479	0.0009	108.1	1.8	108.6	1.0	108.5	2	0.08	0.78	104	405	0.26
oc19c16	0.1129	0.0017	0.0167	0.0002	0.3807	0.0487	0.0007	108.6	1.5	107.0	1.2	107.5	2	1.05	0.31	301	791	0.38
oc19c17	0.1139	0.0020	0.0166	0.0002	0.2665	0.0497	0.0011	109.6	1.8	106.2	1.0	106.7	2	3.26	0.07	186	451	0.41
oc19c18	0.1082	0.0028	0.0168	0.0002	0.2244	0.0464	0.0011	104.4	2.6	107.2	1.3	106.8	2	1.14	0.29	249	550	0.45
oc19c19	0.1094	0.0026	0.0168	0.0002	0.2239	0.0473	0.0011	105.4	2.4	107.5	1.1	107.2	2	0.74	0.39	199	400	0.50
oc19c20	0.1132	0.0035	0.0164	0.0002	0.1822	0.0493	0.0015	108.9	3.2	105.2	1.2	105.4	2	1.34	0.25	81	259	0.31
oc19c21	0.1106	0.0036	0.0166	0.0003	0.2351	0.0484	0.0019	106.5	3.3	106.3	1.6	106.3	3	0.00	0.95	71	216	0.33
oc19c22	0.1106	0.0022	0.0167	0.0002	0.2344	0.0477	0.0010	106.5	2.0	106.7	1.0	106.7	2	0.01	0.93	137	317	0.43
oc19c23	0.1118	0.0027	0.0169	0.0002	0.2376	0.0478	0.0013	107.6	2.5	108.2	1.2	108.1	2	0.07	0.79	86	234	0.37
oc19c24	0.1097	0.0029	0.0171	0.0002	0.2243	0.0466	0.0013	105.7	2.6	109.1	1.3	108.7	2	1.63	0.20	83	259	0.32
oc14B40	0.1119	0.0072	0.0160	0.0004	0.1960	0.0456	0.0016	107.7	6.6	102.2	2.6	102.6	5	0.69	0.41	84	270	0.31
oc14B47	0.1102	0.0054	0.0163	0.0004	0.2706	0.0491	0.0009	106.1	4.9	104.1	2.7	104.4	5	0.16	0.69	212	555	0.38
oc14B48	0.1100	0.0092	0.0167	0.0004	0.1363	0.0463	0.0024	105.9	8.4	106.7	2.4	106.7	5	0.01	0.93	219	518	0.42
oc14B49	0.1094	0.0179	0.0168	0.0010	0.1812	0.0555	0.0023	105.4	16.4	107.1	6.3	107.0	12	0.01	0.92	138	396	0.35
oc14B50	0.1111	0.0118	0.0165	0.0009	0.2589	0.0525	0.0013	106.9	10.8	105.4	5.8	105.7	11	0.02	0.89	100	343	0.29
oc14B51	0.1078	0.0116	0.0161	0.0012	0.3583	0.0493	0.0013	104.0	10.7	103.0	7.9	103.3	15	0.01	0.92	80	264	0.30
oc14B52	0.1084	0.0059	0.0167	0.0005	0.2473	0.0463	0.0010	104.5	5.4	106.7	2.9	106.4	5	0.16	0.69	228	478	0.48
oc14B53	0.1101	0.0168	0.0162	0.0008	0.1635	0.0563	0.0028	106.1	15.4	103.7	5.1	103.9	10	0.02	0.88	104	238	0.44
oc14B54	0.1114	0.0088	0.0165	0.0006	0.2449	0.0492	0.0012	107.3	8.1	105.7	4.1	105.9	8	0.04	0.85	123	366	0.34
oc14a41	0.1098	0.0075	0.0165	0.0005	0.2409	0.0499	0.0014	105.7	6.9	105.6	3.5	105.7	7	0.0	0.99	60	175	0.340
oc14a42	0.1095	0.0098	0.0173	0.0005	0.1493	0.0557	0.0015	105.5	8.9	110.7	2.9	110.4	6	0.3	0.56	73	189	0.387
oc14a59	0.1120	0.0077	0.0172	0.0004	0.1735	0.0512	0.0012	107.8	7.1	110.1	2.6	110.0	5	0.1	0.74	106	308	0.344
oc14a60	0.1091	0.0072	0.0166	0.0004	0.1888	0.0520	0.0012	105.1	6.6	106.3	2.6	106.2	5	0.0	0.85	169	352	0.479
oc14a61	0.1131	0.0075	0.0160	0.0006	0.2660	0.0503	0.0016	108.8	6.8	102.4	3.6	103.2	7	0.9	0.35	92	185	0.498
oc14a62	0.1140	0.0142	0.0163	0.0013	0.3151	0.0522	0.0013	109.6	12.9	104.5	8.1	105.5	15	0.2	0.69	82	221	0.373
oc14a63	0.1041	0.0079	0.0172	0.0006	0.2252	0.0485	0.0011	100.5	7.2	110.1	3.7	108.7	7	1.7	0.19	81	249	0.325
oc14a64	0.1118	0.0115	0.0170	0.0008	0.2201	0.0511	0.0013	107.6	10.5	108.4	4.9	108.3	9	0.0	0.94	72	163	0.444
oc14a65	0.1134	0.0102	0.0165	0.0006	0.2088	0.0563	0.0013	109.1	9.3	105.6	3.9	105.9	8	0.1	0.71	102	224	0.456
oc14a66	0.1126	0.0073	0.0170	0.0005	0.2131	0.0499	0.0012	108.4	6.6	108.5	3.0	108.5	6	0.0	0.99	92	258	0.357
oc14a67	0.1043	0.0089	0.0177	0.0006	0.1857	0.0521	0.0015	100.7	8.1	112.9	3.5	111.6	7	2.2	0.14	60	128	0.470
oc14a68	0.1140	0.0076	0.0160	0.0004	0.1976	0.0569	0.0017	109.6	6.9	102.3	2.7	102.9	5	1.1	0.29	54	185	0.294

Appendix 2. *Chemical abrasion U-Th-Pb ID-TIMS data for zircon fractions from TB369, aplite dyke crosscutting Stoddart porphyry, Stoddart zone.*

	Compositional parameters									Radiogenic isotope ratios								Isotopic ages					
Sample (a)	Wt. mg (b)	U ppm (c)	Th / U (d)	Pb ppm (c)	$^{206}Pb^*$ x10^{-13} mol (e)	mol % $^{206}Pb^*$ (e)	Pb^*/Pb_c (e)	Pb_c (pg) (e)	$^{206}Pb/^{204}Pb$ (f)	$^{208}Pb/^{206}Pb$ (g)	$^{207}Pb/^{206}Pb$ (g)	% err (h)	$^{207}Pb/^{235}U$ (g)	% err (h)	$^{206}Pb/^{238}U$ (g)	% err (h)	corr. coef.	$^{207}Pb/^{206}Pb$ (i)	± (h)	$^{207}Pb/^{235}U$ (i)	± (h)	$^{206}Pb/^{238}U$ (i)	± (h)
TB369																							
TB369 A	0.002	940	0.459	26.8	2.0032	97.46%	12	4.29	728	0.146	0.049126	0.921	0.173084	1.013	0.025553	0.212	0.521	153.86	21.56	162.09	1.52	162.66	0.34
TB369 C	0.002	176	0.301	4.9	0.1793	72.82%	1	5.50	68	0.104	0.051318	11.988	0.086446	12.754	0.012217	0.801	0.960	255.13	275.47	84.19	10.30	78.28	0.62
TB369 D	0.002	319	0.402	6.6	0.4281	92.46%	4	2.87	245	0.129	0.048343	2.848	0.107350	3.033	0.016105	0.253	0.752	116.11	67.13	103.54	2.99	102.99	0.26
TB369 E	0.002	48	0.262	1.2	0.0618	84.34%	2	0.94	118	0.083	0.047803	6.622	0.100835	7.024	0.015299	0.553	0.746	89.55	156.88	97.55	6.53	97.87	0.54

(a) A, B etc. are labels for fractions composed of single zircon grains or fragments; all fractions annealed and chemically abraded after Mattinson (2005).

(b) Nominal fraction weights estimated from photomicrographic grain dimensions, adjusted for partial dissolution during chemical abrasion.

(c) Nominal U and total Pb concentrations subject to uncertainty in photomicrographic estimation of weight and partial dissolution during chemical abrasion.

(d) Model Th/U ratio calculated from radiogenic $^{208}Pb/^{206}Pb$ ratio and $^{207}Pb/^{235}U$ age.

(e) Pb* and Pbc represent radiogenic and common Pb, respectively; mol. % $^{206}Pb^*$ with respect to radiogenic, blank and initial common Pb.

(f) Measured ratio corrected for spike and fractionation only. Daly analyses, based on analysis of NBS-982.

(g) Corrected for fractionation, spike and common Pb; up to 1 pg of common Pb was assumed to be procedural blank: $^{206}Pb/^{204}Pb = 18.50 \pm 1.0\%$; $^{207}Pb/^{204}Pb = 15.50 \pm 1.0\%$; $^{208}Pb/^{204}Pb = 38.40 \pm 1.0\%$ (all uncertainties 1-sigma). Excess over blank was assigned to initial common Pb.

(h) Errors are 2-sigma, propagated using the algorithms of Schmitz and Schoene (2007) and Crowley *et al.* (2007).

(i) Calculations are based on the decay constants of Jaffey *et al.* (1971). $^{206}Pb/^{238}U$ and $^{207}Pb/^{206}Pb$ ages corrected for initial disequilibrium in $^{230}Th/^{238}U$ using Th/U [magma] = 3.

(j) Corrected for fractionation, spike and blank Pb only.

Appendix 3. *LAM ICP-MS U-Pb isotopic analyses of magmatic zircon from andesitic dyke, TB038.*

	measured isotopic ratios							Calculated ages										
Analysis	$^{207}Pb/^{235}U$	1σ err.	$^{206}Pb/^{238}U$	1σ err.	Rho	$^{207}Pb/^{206}Pb$	1σ err.	$^{207}Pb/^{235}U$ Ma	1σ err. Ma	$^{206}Pb/^{238}U$ Ma	1σ err. Ma	Conc. age (Ma)	2σ err. Ma	MSWD of conc.	Prob. of conc.	Th (ppm)	U (ppm)	Ratio Th/U
oc15a54	0.07726	0.00420	0.01209	0.00025	0.18770	0.04786	0.00098	76	4	77	2	77	3	0.23	0.63	184	357	0.52
oc15a56	0.07942	0.00471	0.01192	0.00037	0.25910	0.04826	0.00087	78	4	76	2	77	4	0.07	0.79	1588	2118	0.75
oc15a58	0.07373	0.00395	0.01179	0.00030	0.23491	0.04764	0.00074	72	4	76	2	75	4	0.77	0.38	403	828	0.49
oc15a76	0.07259	0.00454	0.01173	0.00047	0.32263	0.04379	0.00133	71	4	75	3	74	6	0.84	0.36	91	140	0.65
oc15a80	0.07390	0.00604	0.01149	0.00035	0.18634	0.05551	0.00139	72	6	74	2	74	4	0.05	0.83	77	156	0.49
oc15a81	0.07939	0.00810	0.01146	0.00049	0.20786	0.05622	0.00144	78	8	73	3	74	6	0.29	0.59	51	184	0.28
oc15a82	0.07880	0.00361	0.01186	0.00036	0.32732	0.04758	0.00086	77	3	76	2	76	4	0.09	0.76	116	269	0.43
oc15a84	0.08055	0.00584	0.01216	0.00045	0.25793	0.04969	0.00159	79	5	78	3	78	6	0.02	0.89	81	145	0.56
oc15a85	0.07969	0.00528	0.01223	0.00027	0.16918	0.05219	0.00131	78	5	78	2	78	3	0.01	0.92	315	522	0.60
oc15a86	0.08186	0.00482	0.01219	0.00043	0.29643	0.04740	0.00099	80	5	78	3	78	5	0.16	0.69	202	373	0.54
oc15a87	0.07987	0.00506	0.01248	0.00037	0.23485	0.04830	0.00123	78	5	80	2	80	5	0.16	0.69	81	198	0.41
oc15a92	0.07863	0.00496	0.01246	0.00040	0.25542	0.04747	0.00122	77	5	80	3	79	5	0.39	0.53	77	128	0.60
oc15a93	0.07431	0.00574	0.01184	0.00050	0.27551	0.04417	0.00123	73	5	76	3	75	6	0.32	0.57	57	128	0.44
oc15a95	0.08016	0.00387	0.01221	0.00026	0.21782	0.04999	0.00080	78	4	78	2	78	3	0.00	0.98	189	455	0.42
oc15a96	0.07802	0.00348	0.01182	0.00024	0.22845	0.04771	0.00090	76	3	76	2	76	3	0.03	0.87	107	271	0.39
oc15a97	0.07825	0.00526	0.01216	0.00038	0.22987	0.05071	0.00132	76	5	78	2	78	5	0.08	0.78	62	145	0.43
oc15a98	0.07909	0.00553	0.01195	0.00036	0.21683	0.05244	0.00125	77	5	77	2	77	4	0.02	0.90	100	225	0.44
oc15a99	0.07866	0.00593	0.01218	0.00039	0.21275	0.04723	0.00135	77	6	78	2	78	5	0.04	0.84	65	166	0.39
oc15c101	0.07930	0.00874	0.01179	0.00045	0.17331	0.05171	0.00143	77	8	76	3	76	6	0.06	0.81	132	247	0.53
oc15c102	0.07875	0.00532	0.01237	0.00043	0.26020	0.04953	0.00131	77	5	79	3	79	5	0.21	0.65	44	105	0.42
oc15c103	0.08078	0.00284	0.01187	0.00017	0.20002	0.04840	0.00167	79	3	76	1	76	2	1.10	0.29	500	995	0.50
oc15c104	0.08174	0.00428	0.01213	0.00033	0.26297	0.05190	0.00118	80	4	78	2	78	4	0.26	0.61	137	254	0.54
oc15a55	0.08245	0.01881	0.01266	0.00401	0.69473	0.04899	0.00176	80	18	81	26	80	35	0.00	0.97	947	1493	0.63
oc15a78	0.08089	0.01302	0.01170	0.00070	0.18540	0.04675	0.00102	79	12	75	4	75	9	0.11	0.74	495	807	0.61
oc15a79	0.07492	0.00434	0.01230	0.00035	0.24760	0.04390	0.00114	73	4	79	2	78	4	1.71	0.19	76	150	0.50
oc15a83	0.07509	0.00530	0.01290	0.00044	0.23983	0.04457	0.00133	74	5	83	3	81	5	3.20	0.07	77	146	0.53

Appendix 4. *LAM ICP-MS U-Pb isotopic analyses of magmatic zircons from Bow Creek granite, Ridge Zone.*

	Measured isotopic ratios							Calculated ages										
Analysis	$^{207}Pb/^{235}U$	1σ err.	$^{206}Pb/^{238}U$	1σ err.	Rho	$^{207}Pb/^{206}Pb$	1σ err.	$^{207}Pb/^{235}U$ Ma	1σ err. Ma	$^{206}Pb/^{238}U$ Ma	1σ err. Ma	Conc. age (Ma)	2σ err. Ma	MSWD of conc.	Prob. of conc.	Th (ppm)	U (ppm)	Ratio Th/U
oc14B55	0.0717	0.0063	0.0109	0.0006	0.3078	0.0485	0.0014	70	6	70	4	70	7	0.01	0.93	276	619	0.44
oc14B58	0.0679	0.0037	0.0106	0.0003	0.2299	0.0479	0.0010	67	4	68	2	68	3	0.07	0.79	694	1082	0.64
oc14B59	0.0733	0.0049	0.0107	0.0005	0.3195	0.0506	0.0013	72	5	69	3	69	6	0.46	0.50	221	501	0.44
oc14B70	0.0772	0.0078	0.0114	0.0006	0.2624	0.0502	0.0015	76	7	73	4	74	7	0.09	0.76	398	741	0.54
oc14B71	0.0726	0.0055	0.0111	0.0006	0.3399	0.0498	0.0013	71	5	71	4	71	7	0.00	1.00	171	381	0.45
oc14B73	0.0686	0.0083	0.0108	0.0006	0.2454	0.0537	0.0022	67	8	69	4	69	8	0.06	0.80	71	207	0.34
oc14B74	0.0662	0.0038	0.0105	0.0004	0.3186	0.0463	0.0008	65	4	68	2	67	5	0.48	0.49	1057	1295	0.82
oc14B77	0.0696	0.0055	0.0104	0.0003	0.1916	0.0499	0.0015	68	5	67	2	67	4	0.10	0.76	365	684	0.53
oc14B78	0.0703	0.0047	0.0100	0.0004	0.3068	0.0522	0.0013	69	4	64	3	65	5	1.04	0.31	338	591	0.57
oc14B79	0.0722	0.0077	0.0109	0.0006	0.2407	0.0517	0.0014	71	7	70	4	70	7	0.02	0.89	129	332	0.39
oc14B80	0.0663	0.0063	0.0105	0.0004	0.2171	0.0519	0.0014	65	6	67	3	67	5	0.13	0.72	177	409	0.43
oc15a14	0.0668	0.0037	0.0108	0.0003	0.2149	0.0472	0.0011	66	4	70	2	69	3	1.16	0.28	158	367	0.43
oc15a15	0.0624	0.0036	0.0106	0.0003	0.2158	0.0470	0.0010	61	3	68	2	67	3	3.60	0.06	135	335	0.40
oc15a16	0.0683	0.0096	0.0107	0.0006	0.1957	0.0517	0.0012	67	9	68	4	68	7	0.02	0.88	174	378	0.46
oc15a17	0.0697	0.0032	0.0106	0.0002	0.2122	0.0497	0.0009	68	3	68	1	68	3	0.00	0.95	1045	1169	0.89
oc15a18	0.0675	0.0034	0.0107	0.0003	0.2543	0.0458	0.0009	66	3	69	2	68	3	0.59	0.44	209	408	0.51
oc15a19	0.0653	0.0033	0.0105	0.0003	0.2709	0.0456	0.0011	64	3	67	2	67	4	0.98	0.32	139	273	0.51
oc15a21	0.0698	0.0047	0.0109	0.0004	0.2749	0.0496	0.0012	69	4	70	3	69	5	0.06	0.80	123	273	0.45
oc15a22	0.0700	0.0048	0.0105	0.0003	0.2026	0.0483	0.0013	69	5	68	2	68	4	0.05	0.82	338	827	0.41
oc15a35	0.0675	0.0079	0.0108	0.0004	0.1519	0.0548	0.0012	66	8	69	2	69	5	0.17	0.68	264	531	0.50
oc15a36	0.0695	0.0038	0.0108	0.0003	0.2510	0.0489	0.0008	68	4	69	2	69	4	0.08	0.78	429	758	0.57
oc15a37	0.0711	0.0041	0.0109	0.0004	0.3534	0.0449	0.0010	70	4	70	3	70	5	0.00	0.96	195	420	0.46
oc15a38	0.0691	0.0046	0.0108	0.0004	0.2832	0.0475	0.0008	68	4	69	3	69	5	0.12	0.73	153	802	0.19
oc15a39	0.0889	0.0037	0.0114	0.0003	0.3432	0.0531	0.0008	86	3	73	2	75	4	15.73	0.00	780	624	1.25
oc15a40	0.0878	0.0115	0.0113	0.0006	0.2098	0.0680	0.0019	85	11	72	4	73	8	1.46	0.23	37	148	0.25
oc15a41	0.0779	0.0031	0.0116	0.0002	0.2133	0.0508	0.0006	76	3	75	1	75	2	0.32	0.57	79	1380	0.06
oc15a43	0.0725	0.0037	0.0113	0.0002	0.2055	0.0463	0.0008	71	4	73	2	73	3	0.23	0.63	353	560	0.63
oc15a44	0.0727	0.0043	0.0116	0.0003	0.1884	0.0517	0.0010	71	4	74	2	74	3	0.51	0.47	214	426	0.50
oc15a20	0.0937	0.0060	0.0114	0.0005	0.3549	0.0602	0.0013	91	6	73	3	76	6	11.00	0.00	168	357	0.47
oc15a23	0.0657	0.0399	0.0111	0.0018	0.1328	0.0486	0.0019	65	38	71	11	71	23	0.03	0.86	224	426	0.53